

Forschungszentrum Karlsruhe
Technik und Umwelt

Wissenschaftliche Berichte
FZKA 6255

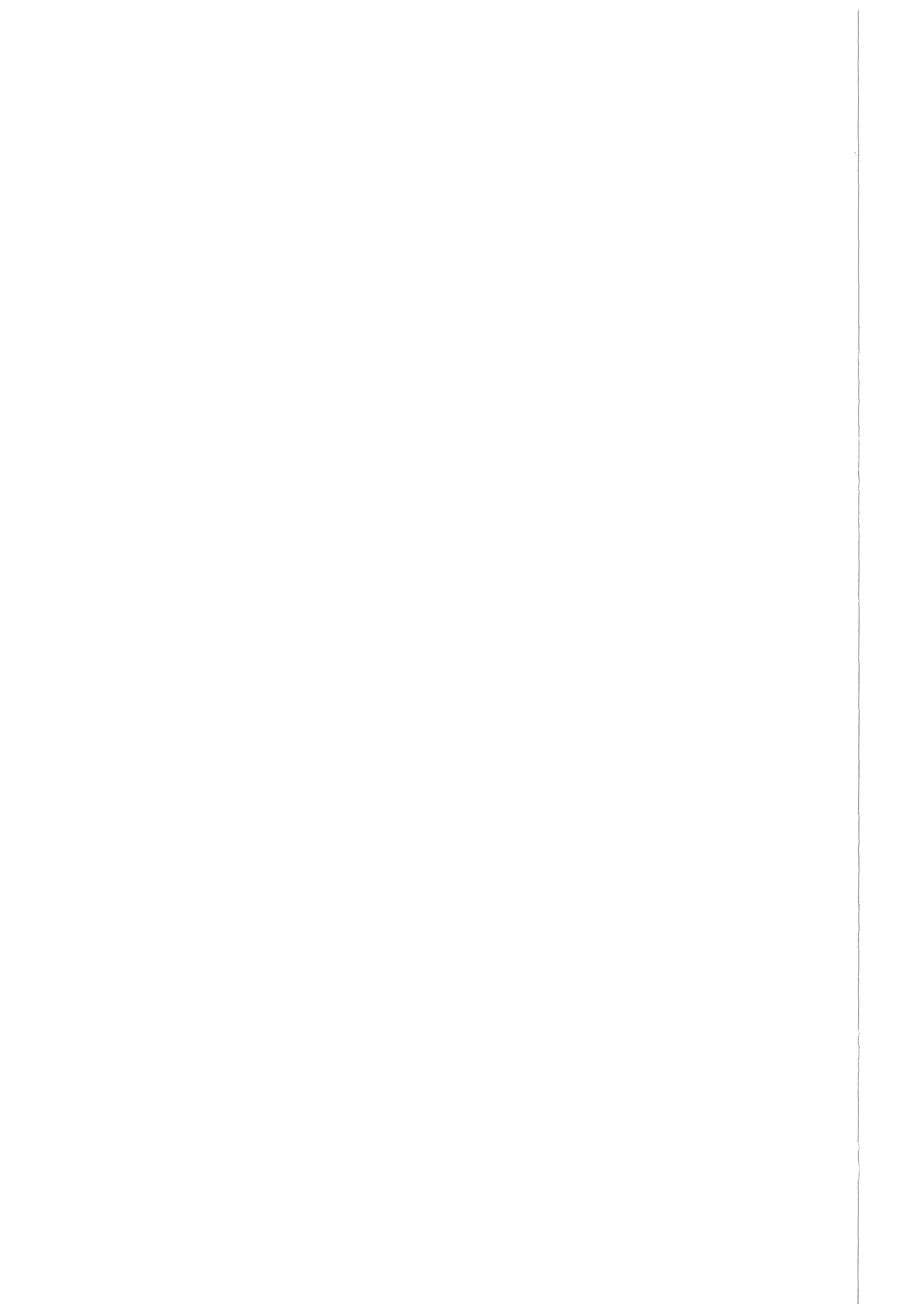
**Support for
ITER ECRF Design**
**Subtask 3: Design and
Optimization of the Window Unit**
– Final Report –

**M. Thumm, O. Braz, C. T. Iatrou,
R. Heidinger, S. Henry, M. Makowski,
R. Spörl, J. Szczesny**

**Institut für Technische Physik
Institut für Materialforschung**

**Projekt Kernfusion
Association EURATOM-FZK**

Februar 1999



Forschungszentrum Karlsruhe
Technik und Umwelt
Wissenschaftliche Bericht
FZKA 6255

SUPPORT FOR ITER ECRF DESIGN

Subtask 3: Design and Optimization of the Window Unit

- Final Report -

M. Thumm¹⁾, O. Braz¹⁾, C.T. Iatrou, R. Heidinger, S. Henry, M. Makowski²⁾, R. Spörl,
J. Szczesny

Institut für Technische Physik
Institut für Materialforschung

Projekt Kernfusion
Association EURATOM-FZK

¹⁾ also Universität Karlsruhe, Institut für Höchstfrequenztechnik und Elektronik

²⁾ ITER Joint Work Site, Max-Planck-Institut für Plasmaphysik, Garching b. München

Als Manuskript gedruckt
Für diesen Bericht behalten wir uns alle Rechte vor
Forschungszentrum Karlsruhe GmbH
Postfach 3640, 76021 Karlsruhe
Mitglied der Hermann von Helmholtz-Gemeinschaft
Deutscher Forschungszentren (HGF)
ISSN 0947-8620

SUPPORT FOR ITER ECRF DESIGN

Subtask 3: Design and Optimization of the Window Unit

- Final Report -

Task-No.: G52 TD 10 FE

ID-No.: GB7 – EU- D351

Executive Summary

The proposed ITER ECH window unit employs a single, edge-cooled (water, e.g. 20°C) CVD-diamond disk in a corrugated HE_{11} waveguide with 52 mm inner diameter, with an outer disk diameter of 77 mm and a thickness of 1.482 mm ($4 \lambda/2$). Thermal computations show that for larger outer disk diameters the peak temperature is unaffected. Thus due to the high thermal conductivity of the diamond, the exposed window edge area does not have to be large to obtain significant heat transfer. This implies that the window diameter can be minimized which has the added benefit of reducing the cost. For a power of 1 MW at 170 GHz, a loss tangent of $1 \cdot 10^{-5}$, a thermal conductivity of 1800 W/mK (at room temperature) and a heat transfer coefficient of 12 kW/m²K (water flow: 13.5 l/min, water velocity: 2 m/s, room temperature) to the cooling water the central window temperature will not be higher than approx. 45°C and the edge temperature is about 30°C. The absorbed power is 176 W. Simulations also show that steady state conditions are generally achieved in under 3 s and that a 2 MW window should be feasible. Owing to the negligible temperature dependence of the CVD-diamond loss tangent, also the approximately 100°C hot torus cooling water could be used to cool the window. Simulations of an "encased" window, a window in which the edge of the disk has been covered with a 0.4 mm thick layer of electrodeposited copper (tritium barrier in case of broken window disk), show that this is feasible without a significant decrease in heat transfer rate.

Neutron irradiation tests were extended to fluences of 10^{21} n/m² ($E > 0.1$ MeV). Even at this damage level (10^{-4} dpa) which corresponds to the recommended upper fluence level for cryogenically-cooled Sapphire windows, no critical radiation enhanced losses were measured at 90 GHz and 145 GHz. No in-beam effects at 800 Gy/s (electrons) and 0.75 Gy/s (X-rays) were observed (see GB7-EU-T246).

Finite element stress calculations also taking into account the brazing/bonding stress show that the maximum principal stress is located in the window brazing (205 MPa) and is always present. During a 0.5 MPa static overpressure event the stress increases to 290 MPa and the transmission of 1 MW microwave power finally increases the stress to 300 MPa. All these stress values are upper limits since a rigid connection between brazing collar and window disk was assumed. Because the ultimate bending strength of white CVD diamond is approximately 600 MPa all stresses are well below the admissible limits.

Metallization/bonding techniques for CVD diamond disks have been developed in collaboration with DeBeers. The elastic properties of a ductile Al-based braze joined by solid-phase diffusion bonding to the diamond disk are used to reduce the thermal stressing as much as possible. The disadvantage of this technique is the relatively low allowed maximum bakeout temperature of the window unit of 450°C (guaranteed by DeBeers). Several test windows were thermally cycled as if they would be installed as a window on a gyrotron. No diffusion degradation of the brazing has been observed. Currently, bonding experiments with Au-based brazing materials are performed in order to allow a bakeout cycle of up to 550°C.

A complete design of the window unit has been performed with the aim to get a compact device. The drawings are available. Considerations on water flow, pressure drop and heat exchange coefficient are included in this report. Modelling experiments using a copper disk equipped with an electrical heater have been performed.

Through the optional use of a double window, window failures could be easily detected (as on the JET LH and ICRH systems). A very high vacuum ($\approx 10^{-9}$ Torr) can be achieved within the interspace between the two window disks. Since the total volume is small, vacuum pumping can be done with only one VAC-Ion pump. Any failure of either window is detectable as a pressure rise on the ion pump even in the case in which a lower grade vacuum ($\approx 10^{-5}$ Torr) is present on the opposing surface. Bandwidth calculation show, that the disk distance should be e.g. 52.9 mm = $30 \cdot \lambda$.

Investigations on windows for step tunable gyrotrons were also undertaken. For this application, a Brewster angle window is used. Prototype quartz and silicon nitride Brewster windows were installed on a gyrotron and used to demonstrate "fine" step tuning ($\Delta f \approx 3.7$ GHz) in a band from 114 to 166 GHz. High output power around 1.5 MW with efficiencies around 50 % (Depressed Collector) has been obtained at all frequencies. It was also demonstrated that the power absorbed by a Brewster window is generally lower than that by a conventional plane window.

BEITRAG ZUM ITER ECRF DESIGN

Subtask 3: Auslegung und Optimierung der Fenstereinheit

- Schlußbericht -

Task No.: G52 TD 10 FE

ID-No.: GB – EU - D351

Kurzfassung

Die für ITER vorgeschlagene ECH-Fenstereinheit verwendet eine mit Wasser (z.B. 20° C) am Rand gekühlte CVD-Diamantscheibe in einem HE₁₁-Rillenhohlleiter mit 52 mm Innendurchmesser. Der Scheibenaußendurchmesser beträgt 77 mm und die Dicke der Scheibe ist 1,482 mm ($4 \lambda/2$). Berechnungen des thermischen Verhaltens zeigen, daß bei Vergrößerung des äußeren Scheibendurchmessers die Spitztemperatur in der Fenstermitte unbeeinflusst bleibt. Aufgrund der hohen Wärmeleitfähigkeit von Diamant muß also der mit Wasser gekühlte Scheibenrand nicht groß sein, um einen signifikanten Wärmetransport zu erhalten. Somit kann der Scheibendurchmesser klein gehalten werden, was außerdem auch noch die Kosten reduziert. Für eine Leistung von 1 MW bei 170 GHz, einen Verlusttangens von $1 \cdot 10^{-5}$, eine Wärmeleitfähigkeit von 1800 W/mK (bei Zimmertemperatur) und einen Wärmeübertragungskoeffizienten von 12 kW/ m²K zum Kühlwasser (Wasserfluß: 13,5 l/min, Wassergeschwindigkeit: 2 m/s, Zimmertemperatur) ist die Temperatur im Zentrum des Fensters nicht höher als ungefähr 45°C und die Randtemperatur ca. 30°C. Die absorbierte Leistung ist 176 W. Die Simulationsrechnungen zeigen auch, daß das Gleichgewicht in unter 3 Sekunden erreicht wird und daß ein 2 MW-Fenster machbar ist. Aufgrund der vernachlässigbaren Temperaturabhängigkeit des Verlusttangens von CVD-Diamant kann ebenso das 100°C heiße Toruskühlwasser zur Fensterkühlung verwendet werden. Simulationsrechnungen für eine Fensterscheibe, deren Kühlrand mit einer 0,4 mm starken, galvanischen Kupferschicht eingekapselt ist, so daß im Falle eines Scheibenbruchs eine Tritiumbarriere gegeben ist, zeigen, daß dadurch der Wärmefluß nicht signifikant verkleinert wird.

Es wurden Bestrahlungstests von Neutronen bei einer erhöhten Fluenz von 10^{21} n/m² ($E > 0,1$ MW) durchgeführt. Selbst bei diesem Bestrahlungsmaß (10^{-4} dpa), das der für kryogen gekühlte Saphirfenster empfohlenen oberen Fluenzgrenze entspricht, wurden bei 90 GHz und 145 GHz keine kritischen, durch Strahlung induzierte erhöhten Verluste gemessen. Bei 800 Gy/s (Elektronen) und 0,75 Gy/s (Röntgenstrahlung) wurden keine "In-Beam"-Effekte beobachtet (siehe auch GB7-EU-T246).

Finite-Elemente-Berechnungen der mechanischen Spannungen, unter Mitberücksichtigung der Spannung an der Lötverbindung zeigen, daß der Hauptanteil der Spannung genau an dieser Lötverbindung auftritt (205 MPa) und deswegen stets vorhanden ist. Im Falle eines Störfalls mit 0,5 MPa Überdruck würde die maximale Spannung auf 290 MPa ansteigen und die zusätzliche Transmission von 1 MW Mikrowellenleistung würde schließlich zu 300 MPa führen. Alle diese Werte der mechanischen Spannung sind obere Grenzen, da eine starre Verbindung zwischen Lötkragen und Fensterscheibe angenommen wurde. Da die maximal zulässige Biegespannung von CVD-Diamant 600 MPa beträgt, sind alle Spannungen unterhalb der erlaubten Grenzen.

Metallisierungs- und Lötversuche wurden in Zusammenarbeit mit DeBeers durchgeführt. Die elastischen Eigenschaften von dehnbaren, auf Aluminium basierenden Lötverbindungen zusammen mit einer "Solidphase diffusion"-Verbindung führen zu einer deutlichen Reduktion der thermischen Spannungen bei CVD-Diamant-Scheiben. Der Nachteil dieser Verbindung stellt die relativ niedrige maximale Ausheiztemperatur von lediglich 450°C (garantiert von DeBeers) dar. Mehrere Testfenster wurden demselben Ausheizzyklus, wie er bei Gyrotrons üblich ist unterzogen. Hierbei konnten keine diffusionsbedingten Änderungen der Lötverbindung festgestellt werden. Zur Zeit werden Metallisierungs- und Lötversuche mit auf Gold basierenden Loten durchgeführt, die eine höhere Ausheiztemperatur von 550°C erlauben.

Eine vollständige Auslegung der Fenstereinheit wurde mit dem Ziel einer kompakten Anordnung durchgeführt und die technischen Zeichnungen wurden erstellt. Betrachtungen zum Wasserfluß, Druckabfall und Wärmeübertragungskoeffizienten sind in diesem Bericht enthalten. Es wurden Modellexperimente mittels einer mit einem elektrischen Heizer ausgestatteten Kupferscheibe durchgeführt.

Durch den ebenfalls möglichen Einsatz eines Doppelscheibenfensters könnten Fensterfehler einfach nachgewiesen werden (wie bei den JET LH und ICRH Systemen). Im kleinen Volumen zwischen den beiden Scheiben könnte mit einer einzigen "VAC-Ion"-Pumpe ein hohes Zwischenvakuum ($\approx 10^{-9}$ Torr) erreicht werden. Jeder Bruch einer der beiden Scheiben könnte dann durch den Druckanstieg in der Ionengetterpumpe nachgewiesen werden. Dies gilt auch für die Torusseite wo das Vakuum ca. 10^{-5} Torr beträgt. Betrachtungen zur Bandbreite zeigen, daß der Scheibenabstand, z.B. $52,9 \text{ mm} = 30 \cdot \lambda$ sein sollte.

Untersuchungen zu Fenstern für stufenweise frequenzdurchstimmbare Gyrotrons wurden ebenfalls durchgeführt. Für diese Anwendungen wird eine Brewsterfenster eingesetzt. Prototyp Brewsterfenster aus Quarz und Siliziumnitrid wurden in ein Gyrotron eingebaut und damit eine "Feindurchstimmung" ($\Delta f \approx 3,7 \text{ GHz}$) im Frequenzband von 114 bis 166 GHz demonstriert. Bei allen Frequenzen wurden Ausgangsleistungen von ca. 1,5 MW mit einem Wirkungsgrad um 50 % (Depressed Collector) erzielt. Es wurde ebenfalls gezeigt, daß die in einem Brewsterfenster absorbierte Leistung im allgemeinen niedriger als bei einem entsprechenden konventionellen, ebenen Fenster ist.

Contents

Executive Summary

Kurzfassung

1.	Introduction	1
2.	Permeation of Tritium through Window Materials	6
3.	Edge-Cooled CVD-Diamond Window	6
3.1	Thermal Finite Element Calculations	11
3.2	Finite Element Calculations on Stresses	13
4.	Design of Window Block	17
5.	Cooling Modelling Experiments	26
6.	Broadband ECH Systems	28
	Acknowledgments	37
	References	38

1. Introduction

Electron Cyclotron Heating (ECH) is one of the major candidates for Heating and Current Drive (H&CD) on ITER. ECH is extremely attractive from a reactor engineering point of view, offering compact launch structures, high injected power density (10 MW/m²), and a simple interface with the shield/blanket. High unit power, in excess of 1 MW, and high-efficiency gyrotrons significantly reduce the system cost by reducing the size of the auxiliary support systems (power supplies, cooling, input power, ...). CW operation is required for some of the anticipated ITER applications: 3 s for start-up, 100 s for heating to ignition and 100-1000 s for current drive. In order for the Electron Cyclotron System to perform these functions a window must be developed to serve as both the tritium containment barrier on the torus and as the output window on the gyrotron. The former application is technically more demanding because a torus window must also serve as a reliable confinement barrier, should not use FC-cooling liquid, must not degrade unacceptably under modest neutron and γ irradiation (and X-rays) and in the case of cryo-cooling must be prevented by a cold trap from cryo-pumping. Part of the safety function is that it withstand a 0.5 MPa static overpressure during off-normal events. The objective of the present research activity is to develop in continuation of the ITER Task GB-EU-D321 a torus window unit design and specification.

The ECH system layout with multi-beam launchers [1,2] applies the concept of the integrated modular equatorial port design which favours standardization and interchangeability. The level of standardization is being further increased as the design progress and common mechanical components, structures and auxiliaries are being designed for three different radio frequency systems.

The launcher design incorporates a monolithic port-plug assembly (Fig. 1) with ceramic windows located at the main flange of the vacuum vessel port (Fig. 2), to provide the primary containment boundary, and similar mechanical interfaces with the vacuum vessel. The port plug is composed of nuclear shielding and power transmission components together with the mechanical assemblies needed to support these structures. The plug features an all-metal construction, does not extend ITER vacuum boundaries, fits within a standard remote handling transport cask and is designed to be assembled and disassembled in the hot-cell.

The radial control of the location of the power deposition is obtained through oblique launch of the wave in the toroidal direction. Extensive modelling has shown that the launch of a single frequency (170 GHz), elliptically polarized, ordinary mode wave from the low-field-side is sufficient for both heating and current drive, over a wide range of fields (4.0- 5.7 T), provided that a modest steering capability is incorporated in the launcher design.

Two equatorial ports are used to inject 50 MW of EC power for both heating and current drive. The same two ports are also used for the EC start-up and wall conditioning system with one 3 MW system installed per port. The launch configuration is consistent with the requirements for start-up and wall conditioning although in this case, frequencies in the range 90-140 GHz are used and steerable injection is not strictly needed. An upgrade to a total ~80 MW of injected power (40 MW/port) is possible without increasing the number of ports.

Power is injected into the torus through 7 slots in the shield-blanket by means of steerable mirrors, located behind the shield-blanket. Each row of 7 mirrors is actuated individually. An array of 49 (7 x 7) corrugated circular HE₁₁ waveguides feeding the mirrors are offset relative to the slots in order to reduce direct neutron streaming which is further reduced by a double miter-bend assembly introduced in the waveguide run and sandwiched between segmented blocks of shielding to form a

shielded labyrinth ("dog-leg"). Compared to the first design (GB-EU-D321) more shielding is added and access to the interspace is possible. The waveguide runs continue to the closure plate at the back of the equatorial port. Evacuated corrugated circular HE_{11} waveguides are used for power transmission from the gyrotrons to the torus vessel.

The ITER window block resides at the boundary between in-vessel and ex-vessel systems and consequently forms the containment boundary for the ECH systems. Its design must be consistent with the general ITER design principles and machine constraints (port size, vacuum, etc.) and should address the major interfaces involving:

(i) safety and shielding

- vacuum leak detection methodology
- it must withstand a static 0.5 MPa pressure
- it forms the primary tritium containment boundary
- both mechanical and microwave performance must not be severely degraded by neutron and γ -radiation

(ii) cooling

(iii) maintenance and remote handling.

DIMENSIONS RELATE TO ROOM TEMPERATURE (293K)

VACUUM VESSEL

BLANKET MODULE

BLANKET BACKPLATE

VACUUM VESSEL
EQUATORIAL PORT
EXTENSION

VACUUM VESSEL
PRIMARY CLOSURE PLATE

WAVEGUIDE

ATTACHMENT STRUCTURE

SHIELDING SUPPORT STRUCTURE

FIXED MIRROR

STEERABLE MIRROR

FLEXIBLE PLATE ATTACHMENT

SHIELDING

SLOTTED SHIELD BLANKET MODULE

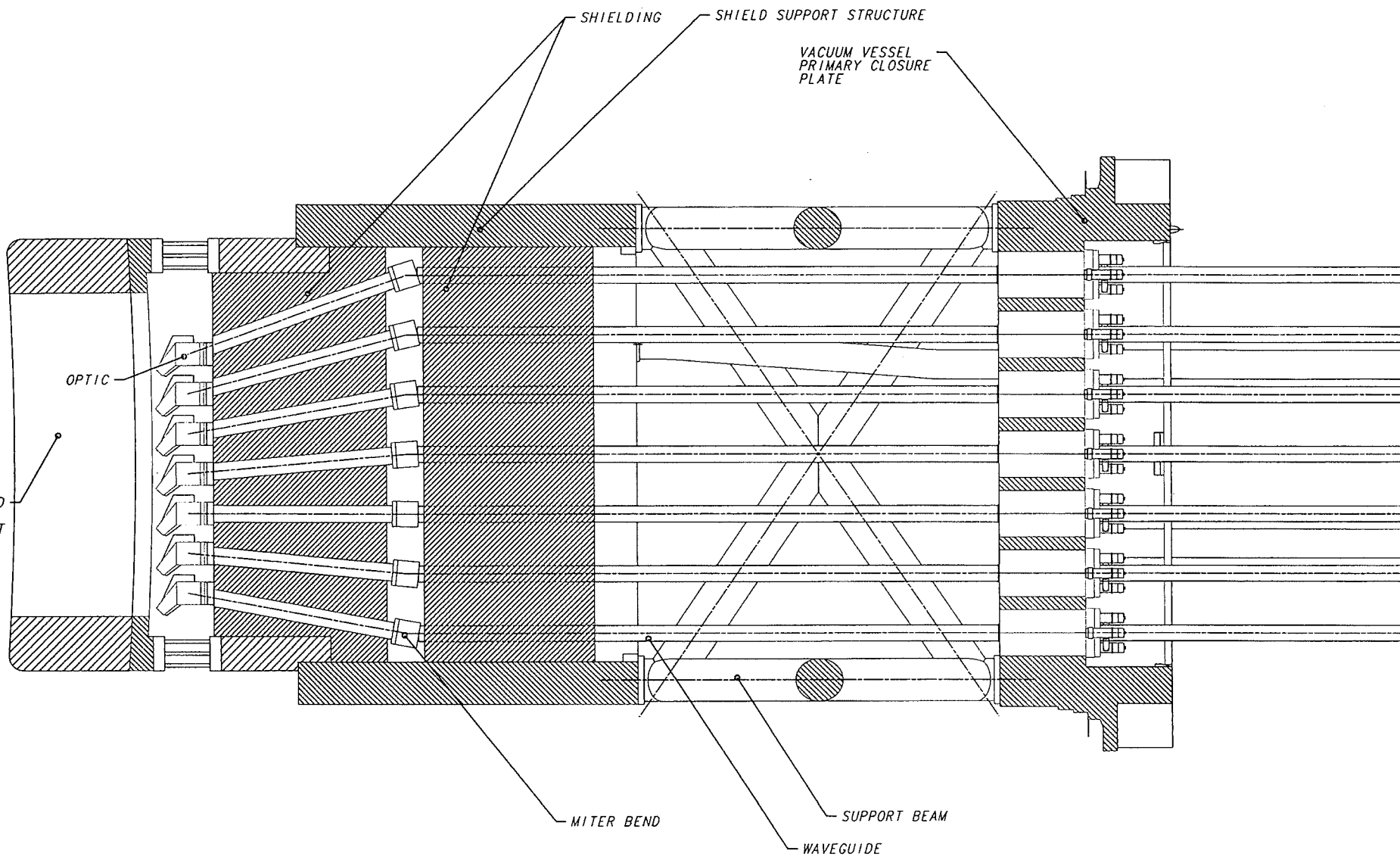
Fig. 1: Isometric view of the ITER-ECH launcher.

ONLY GEOMETRY RELATING TO THE DRAWING WBS IS TO BE USED.

TITLE ECH&CD PORT PLUG ASSEMBLY ISO VIEW		DRG FRAME SIZE 840 x 594		ITER-EDA		 <p>INTERNATIONAL THERMONUCLEAR EXPERIMENTAL REACTOR</p>
DATE 03-JUN-98	WORK BREAKDOWN STRUCTURE 5.2	DRAWN B.D. CHE'D	D.O.W	RESP. ENGR JCM	RESP. OFFR JCM	
BASILINE VERSION -	W.B.S. TITLE Electron Cyclotron Heating & Current	REV. ENGR JWS	CHE'D	RESP. OFFR	NAME OF ORGANISATION GARCHING JWS	The information on this drawing is confidential under the terms of the ITER EDA agreement. This information shall not be transmitted to anyone who is not authorized to receive it.
DO NOT TAKE MEASUREMENTS USE ONLY DIMENSIONS GIVEN		THIRD ANGLE PROJECTION		DRAWING NUMBER 5.210.06910.00.7		PROJECT FROM THE ITER EDA AGREEMENT

DIMENSIONS RELATE TO ROOM TEMPERATURE (293K)

Fig. 2:
Plan view of the ITER-ECH antenna
port plug assembly.



NOTES.
1/. ALL DIMENSIONS IN
millimetres UNLESS STATED

ONLY GEOMETRY RELATING TO THE DRAWING WBS IS TO BE USED.

0 100 500 1000		DRC FRAME SIZE #40 x 594		ITER-EDA		 <p>INTERNATIONAL THERMONUCLEAR EXPERIMENTAL REACTOR</p>
TITLE ECH&CD PORT PLUG ASSEMBLY PLAN VIEW WITHOUT PORT		DRAWN D.O. CHK'D D.O.W.	NOT FOR PUBLICATION		<p>The information on this drawing is confidential under the terms of the ITER EDA agreement. This information shall not be transmitted to anyone who is not authorized to receive it.</p>	
DATE 03-JUN-98	WORK BREAKDOWN STRUCTURE 5.2	BPD JCM JCM	RESP. ENGR JWS CHK'D RESP. OFFER	NAME OF ORGANISATION		
BASELINE VERSION -	W.B.S. TITLE Electron Cyclotron Heating & Current	M/M	M/M	GARCHING JWS		
DO NOT TAKE MEASUREMENTS USE ONLY DIMENSIONS GIVEN		THIRD ANGLE PROJECTION		DRAWING NUMBER	SCALE 1/1	
				5.20.0.6.910.0.0.1	2.0.0.0.0.3W	

Three different options for the interspace region are in discussion (Fig. 3), (1) double window with isolation valve to gyrotron, (2) gate valve, single window, isolation valve, (3) gate valve, two windows, isolation valve.

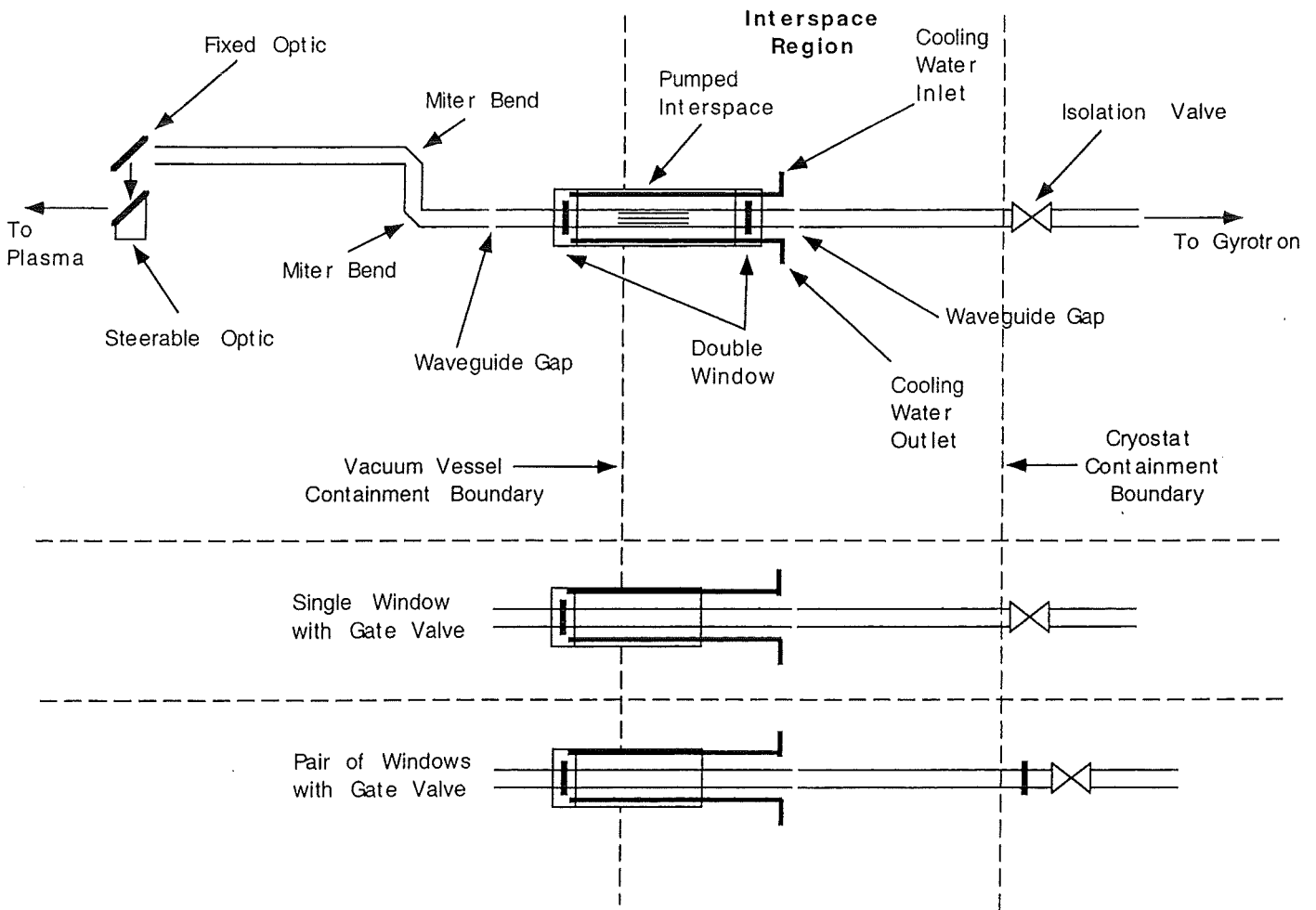


Fig. 3: Options for the interspace region.

2. Permeation of Tritium through Window Materials

The permeation of tritium through mm-wave window materials is a so called gas driven permeation (GDP) of T_2 molecules. The molecules are adsorbed at the window disk surface, thus must be dissociated to tritium atoms which finally diffuse into the bulk material, resulting in comparatively low penetration efficiency. Form of window material (e.g. single-crystal, poly-crystalline, α -, β -, sintered) and impurity levels can have a large effect on the specimen permeability. The tritium diffusion coefficient of MgO-doped poly-crystalline Al_2O_3 is more than 3 orders of magnitude larger than for pure Al_2O_3 . The difference in the diffusion coefficient of single-crystal α and β SiC is roughly 1 to $\frac{1}{2}$ orders of magnitude. Up to now no measurements for chemical vapor deposition (CVD) diamond have been published. The measured permeation coefficients of ceramics for hydrogen are drastically lower than those for metals [3,4]. For example, at a temperature of 500 K, the permeation coefficient of alumina is, respectively, 10^{15} , 10^{18} and 10^{20} times lower than that of tungsten, gold and stainless steel. This means that probably the weakest element of the window for tritium permeation is the brazing/bonding collar and not the disk.

3. Edge-Cooled CVD-Diamond Window

A water-cooled window has the two very important advantages, that it is employing a cheap and effective coolant and it is compact, simple and likely more reliable as other solutions and thus can be also easily used as torus window.

As a potential new material for non-cryogenically cooled high-power mm-wave windows, CVD diamond is very attractive due to its outstanding mechanical strength properties, modest dielectric constant, low loss tangent and phenomenal thermal conductivity at room temperature [5-7]. Current CVD capabilities have allowed for tests with samples of up to 120 mm diameter and 2.2 mm thickness at $f = 145$ GHz [9-14]. Manufacturers (DeBeers, FhG-IAF) claim, that they also can produce samples of up to 160 mm diameter. DeBeers company has already manufactured several disks of about 100 mm diameter and around 2 mm thickness. The current price of such a disk is 70,000 – 100,000 US\$. The loss tangent and permittivity values of these large diameter disks are approximately $2 \cdot 10^{-5}$ and 5.67, respectively, both being nearly constant between 70 K and 370 K. The thermophysical, mechanical and dielectric parameters of CVD diamond in comparison to sapphire are given in Table I together with the related thermal load-failure resistance and power transmission capacities. For comparison, the LN_2 -edge-cooled sapphire window of the European 118 GHz TTE gyrotron (0.5 MW, 210 s), that operates close to the allowable lower limits of these two parameters, has $R'=130$ and $P_r=80$.

Neutron irradiation tests were extended to fluences of 10^{21} n/m² ($E > 0.1$ MeV). Even at this damage level (10^{-4} dpa) which corresponds to the recommended upper fluence level for cryogenically-cooled Sapphire windows, no critical radiation enhanced losses were measured for CVD diamond at 90 GHz and 145 GHz. No in-beam effects at 800 Gy/s (electrons) and 0.75 Gy/s (X-rays) were observed (see GB7-EU-T246).

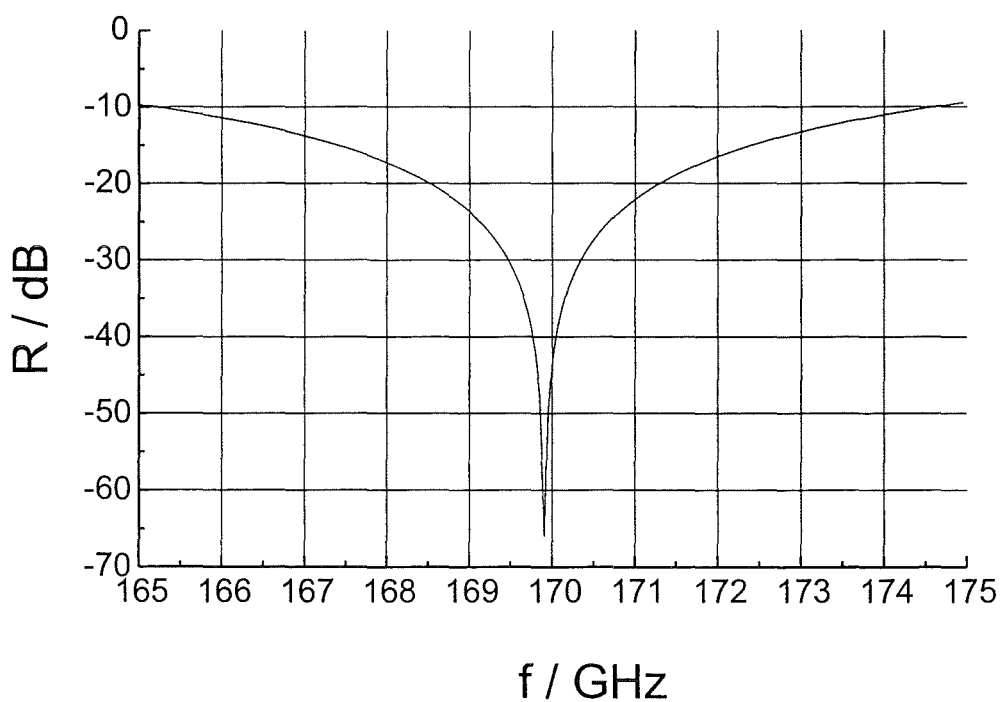
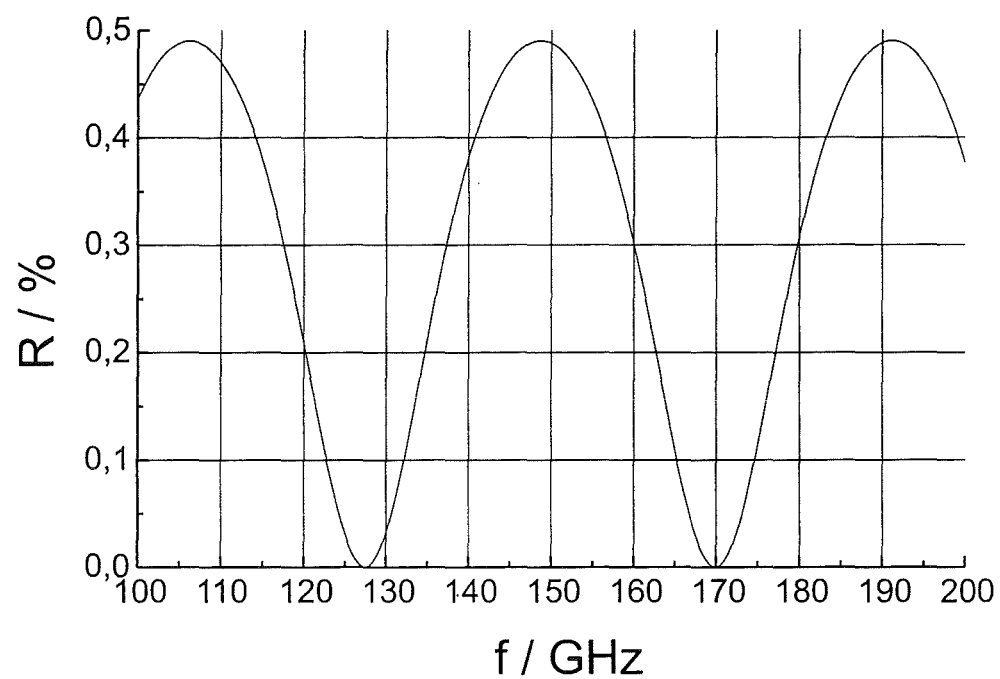
Numerical calculations at 170 GHz (HE_{11} mode) on the temperature and stress distribution have been performed using the finite element code ABAQUS supported by the pre-processor code FEMGEN for preparation of the discretization mesh. The assumed window disk has a waveguide aperture of 52.0 mm diameter with a rim for water edge cooling at 293 K. The thickness is 1.482 mm ($4 \cdot \lambda/2$ in CVD diamond). The 1%-reflection bandwidth is $\Delta f = 2.7$ GHz (Fig. 4). The calculations use the temperature dependences of the diamond material parameters presented in Figs. 5 and 6. The heat transfer coefficient to the cooling water is assumed to be 12 kW/m²K (flow velocity = 2 m/s, room temperature).

Tab. I

Thermophysical, Mechanical and Dielectrical Parameters of Window Materials related to Thermal Load -Failure Resistance and Power Transmission Capacity of Edge-Cooled Windows at Room Temperature (p.c.=poly-crystalline, s.c.=single-crystalline)

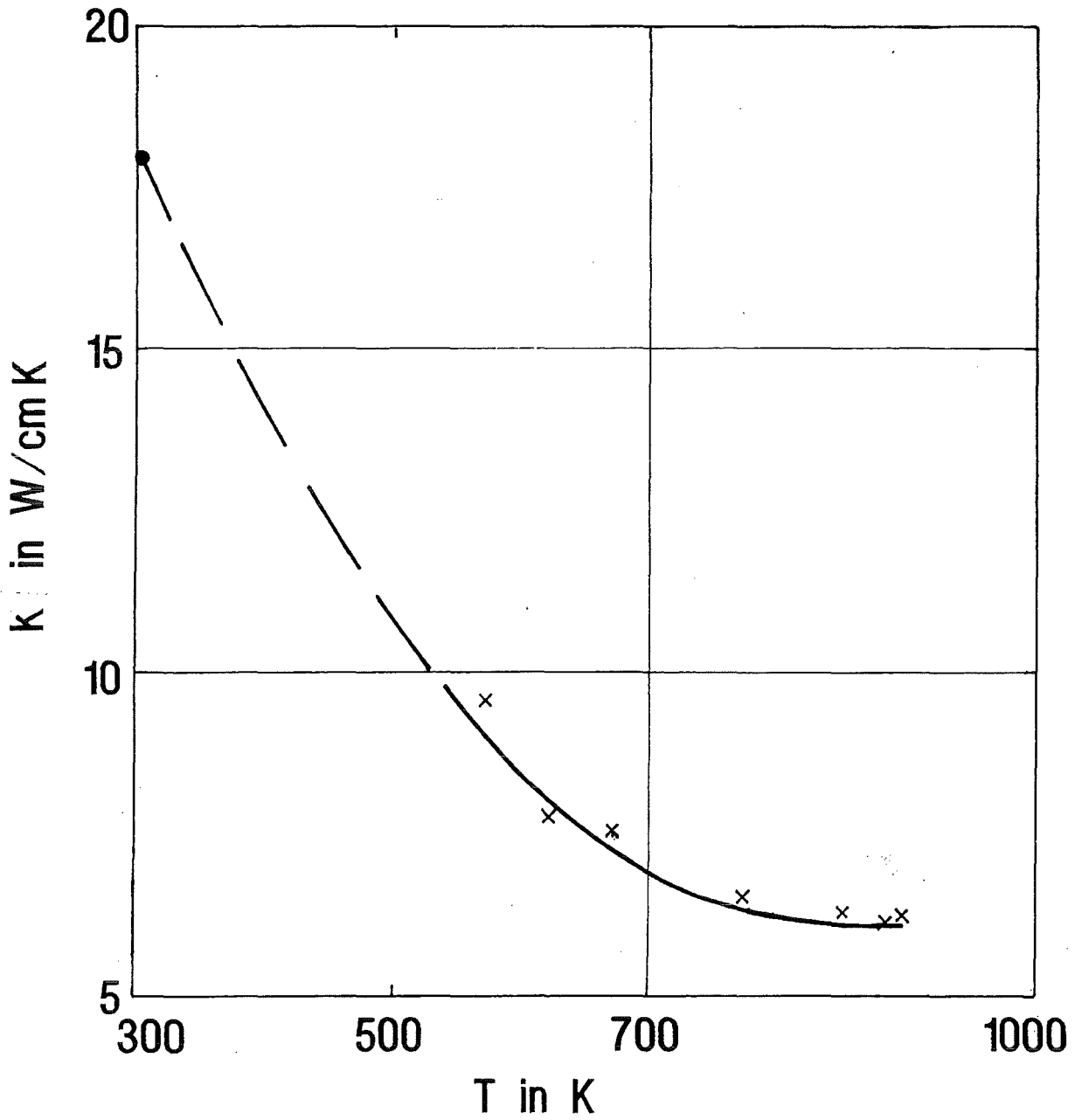
Material	Sapphire (Al ₂ O ₃) s.c.	Diamond (CVD) p.c.
Thermal Conductivity k [W/mK]	40	2000
Ultimate Bending Strength σ_B [MPa]	410	600
Poissons Number ν	0.22	0.1
Density ρ [g/cm ³]	4.0	3.5
Specific Heat Capacity c_p [J/g K]	0.8	0.5
Young's Modulus E [GPa]	385	1050
Therm. Expans. Coeff. α [10 ⁻⁶ /K]	5.5	1.2
Permittivity (145 GHz) ϵ_r'	9.4	5.67
Loss Tangent (145 GHz) $\tan\delta$ [10 ⁻⁵]	20	2
Metallizing/Brazing	o.k.	o.k.
Bakeout Temperature	550°C	550°C
Possible Size \varnothing [mm]	270	120
Cost	high	high
Failure Resistance R' $R' = k\sigma_B (1-\nu)/E\alpha$	6.0	815
RF-Power Capacity P _T $P_T = R'\rho c_p / ((1+\epsilon_r')\tan\delta)$	0.09	107
Radiation Sensitivity n(10 ²⁰ -10 ²¹ n/m ²) γ/X (0.75 Gy/s)	no no	no no

Reflectivity of 1.482 mm diamond window



$$d = 1.482 \text{ mm}; \varepsilon_r = 5.67; \tan\delta = 6 \cdot 10^{-6}$$

Fig. 4: Frequency dependence of the reflectivity of the CVD-diamond.



Thermal conductivity of CVD-Diamond 876 μm ; preliminary
 x Laserflash
 • photoacoustic, needs further investigation

Fig. 5: Temperature dependence of thermal conductivity k of CVD-diamond (B. Schulz and M. Rohde, FZK).

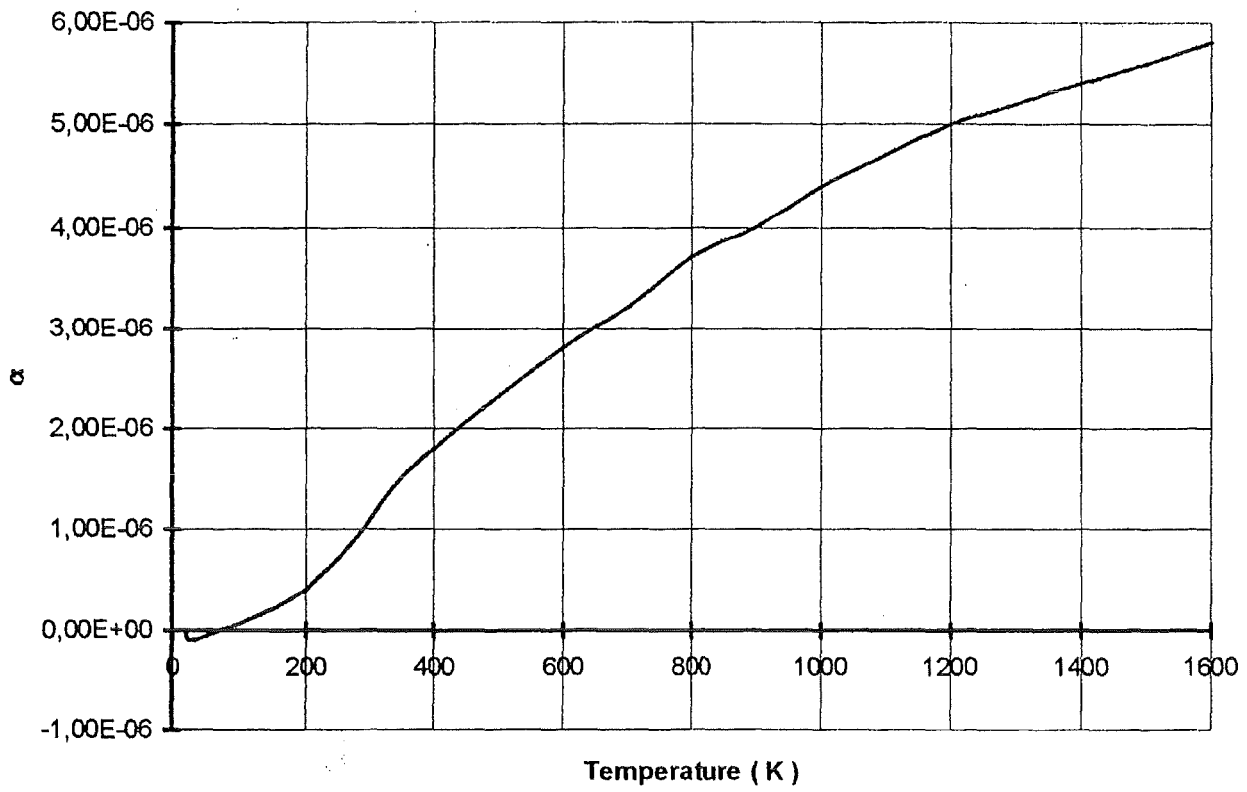


Fig. 6: Temperature dependence of thermal expansion coefficient α of diamond [17].

3.1 Thermal Finite Element Calculations

Figure 7 shows the maximal (center) and minimal (edge) temperature of the diamond disk in dependence of the width of the cooling rim at a mm-wave power of 1 MW for $\tan\delta = 1 \cdot 10^{-5}$. As we can easily see, a cooling rim of about 3 mm width is sufficient to get a maximum center temperature of only around 318 K (45 °C) and an edge temperature of not more than 303 K (30 °C) The corresponding time dependence is plotted in Fig. 8. The power absorbed in the disk is 176 W. Figure 9 presents the maximum and minimum temperatures in dependence of the transmitted power showing that the power capability is even higher than 1 MW.

Simulations of an "encased" window, a window in which the edge of the diamond disk has been covered with a 0.4 mm thick layer of electrodeposited copper, as a tritium barrier and in order to prevent leakage of water into the vacuum in the event of a failed window disk, show that this is feasible without a significant decrease in heat transfer rate. The temperature increase in the disk is lower than 2 °C. The window temperature does not increase significantly with the added thermal resistance of the copper layer due to the extremely high thermal conductivity of diamond.

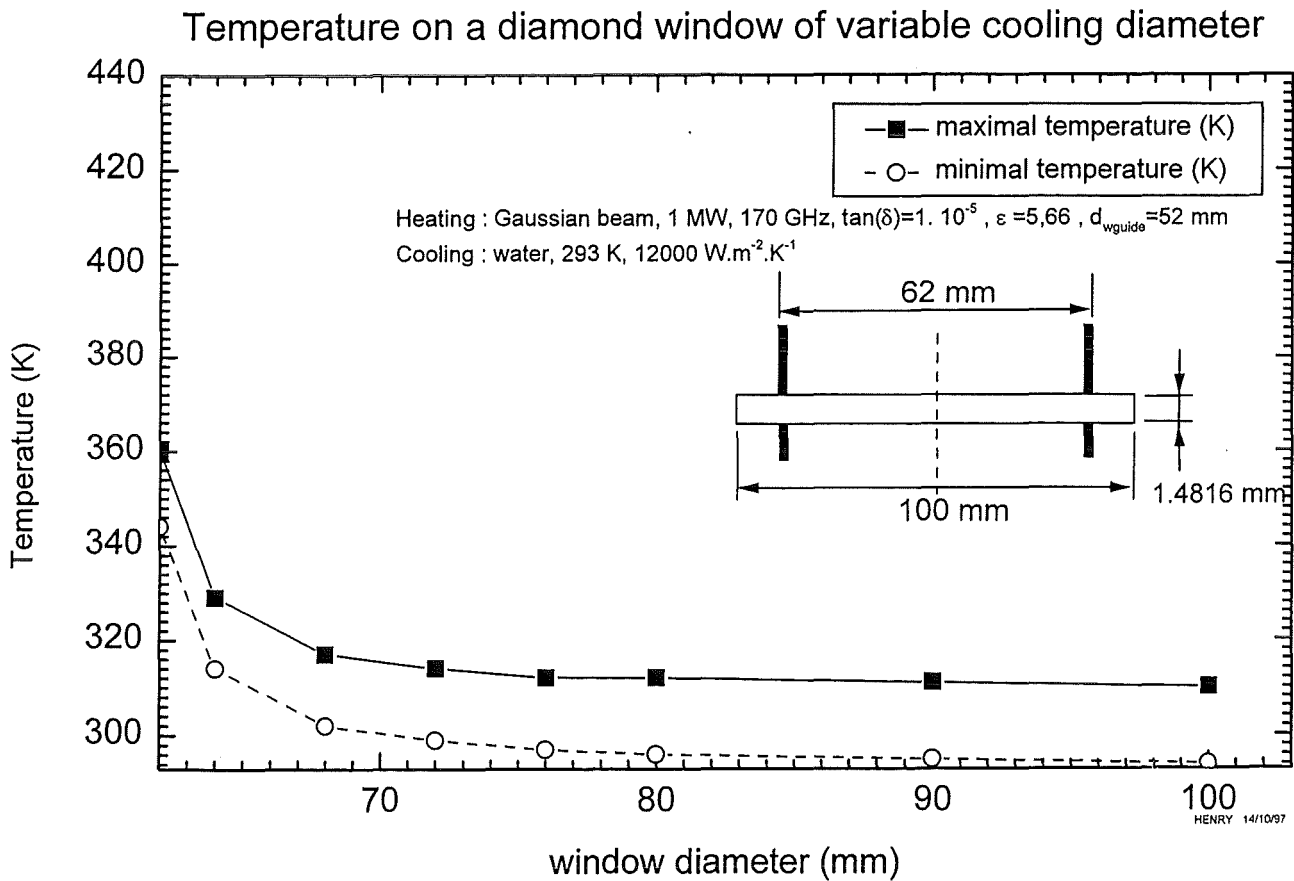


Fig. 7: Dependence of center and edge temperature of CVD-diamond window on the width of the applied cooling rim at 1 MW mm-wave power.

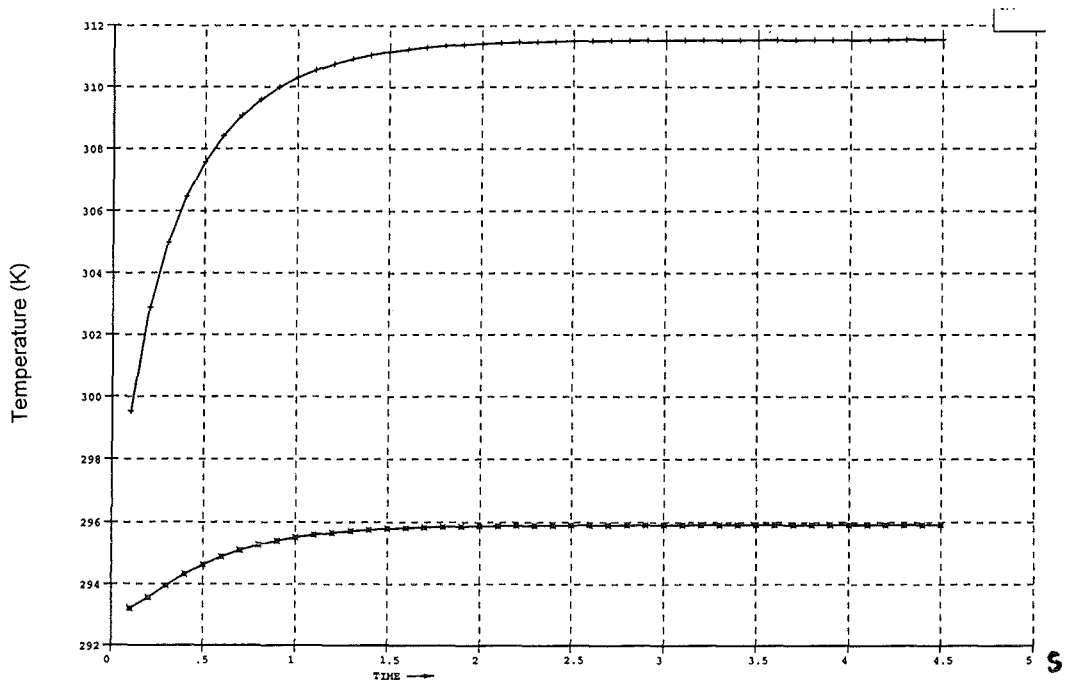


Fig. 8: Time dependence of center and edge temperature of CVD-diamond window disk (80 mm outer diameter) at 1 MW-mm-wave power.

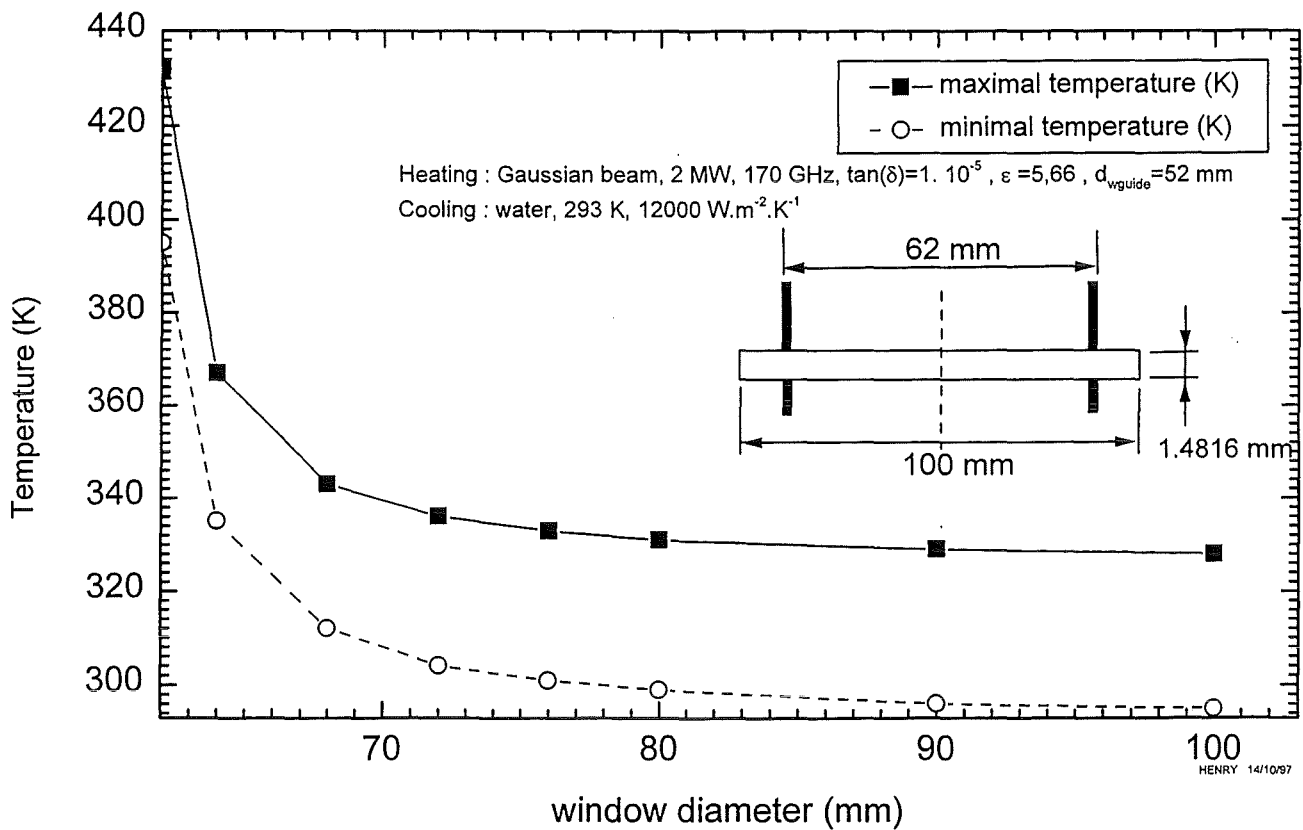
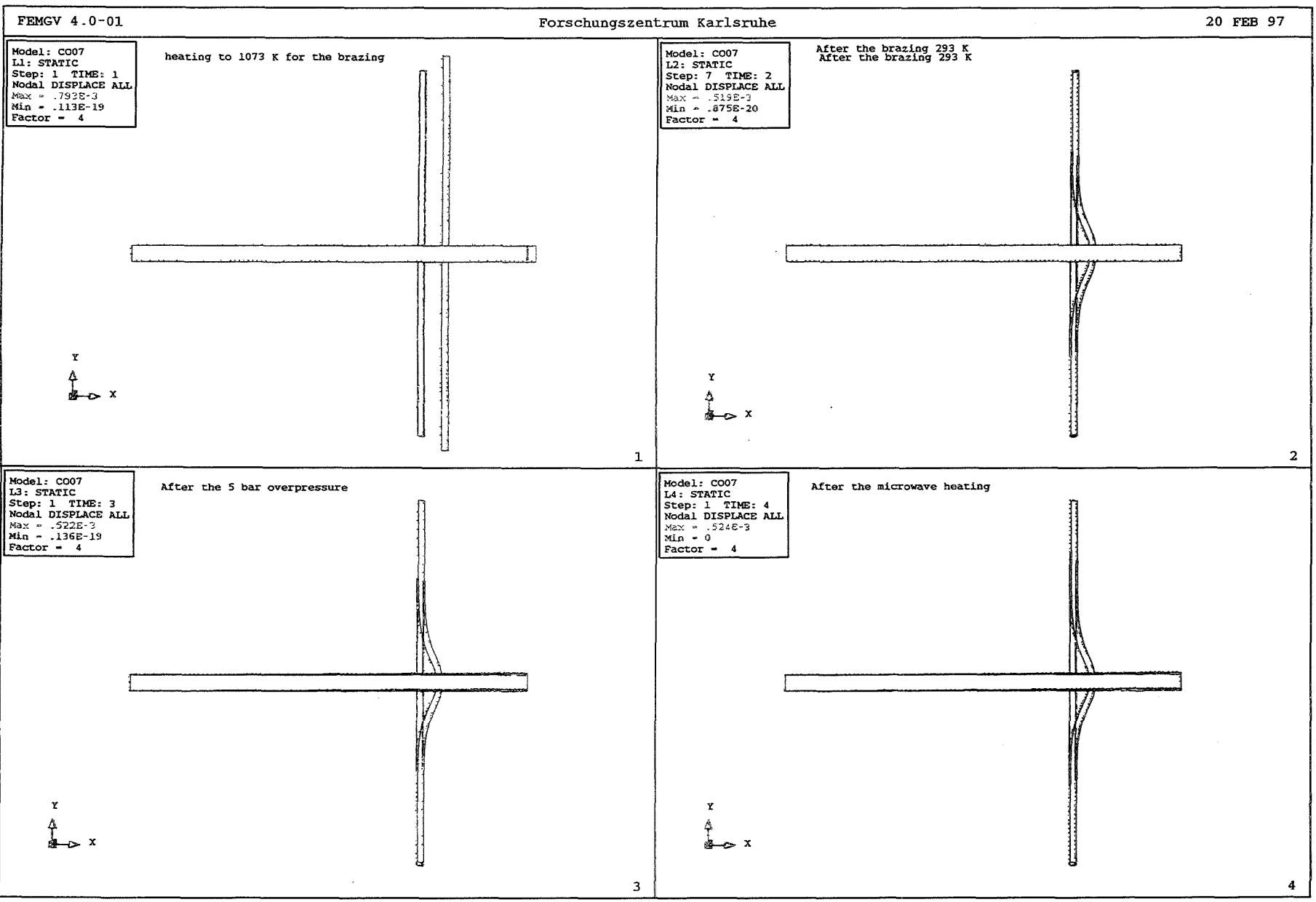


Fig. 9: Dependence of center and edge temperature of CVD-diamond window on the width of the applied cooling rim at 2 MW mm-wave power.

3.2 Finite Element Calculations on Stresses

Metallization/bonding techniques for CVD diamond disks have been developed in collaboration with DeBeers. The elastic properties of a ductile Al-based braze joined by solid-phase diffusion bonding to the diamond disk are used to reduce the thermal stressing as much as possible. The disadvantage of this technique is the relatively low allowed bakeout temperature of the window unit of 450°C (guaranteed by DeBeers). Several test windows were thermally cycled as if they would be installed as a window on a gyrotron. No diffusion degradation of the brazing has been observed. Currently, we are performing bonding experiments with Au-based brazing materials in order to allow a bakeout cycle of up to 550°C.

Finite element (FE) stress calculations also taking into account the brazing/bonding stress show that the maximum principal stress arises from the differential thermal expansion when bonding diamond to copper (205 MPa) and is always present. The differential displacement is around 0.5 mm (Fig. 10). Copper, brazed at 800 °C, is chosen as metal (0.7 mm thick waveguide sleeves) because it is a very plastic and soft material (thermal expansion coefficient: $\alpha = 16.5 \cdot 10^{-6}$ at 293 K). During a 0.5 MPa static overpressure event the maximum stress increases to 290 MPa and the transmission of 1 MW mm-power finally increases the maximum stress to 300 MPa (Figs. 11 and 12). The deflexion of the disk center is approximately 0.05 mm. All these stress values are upper limits since a rigid connection between brazing collar and window disk was assumed. Because the ultimate bending strength of white CVD-diamond is approximately 600 MPa all stresses are below the admissible limits.

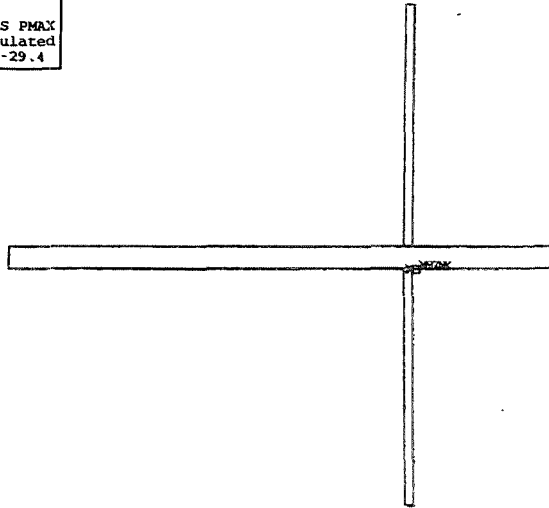


Global displacements (copper, 0.7mm, 20mm)

Fig. 10: Displacement of CVD-diamond disk after brazing, at 0.5 MPa (5 bar) static overpressure and with additional 1 MW mm-wave heating.

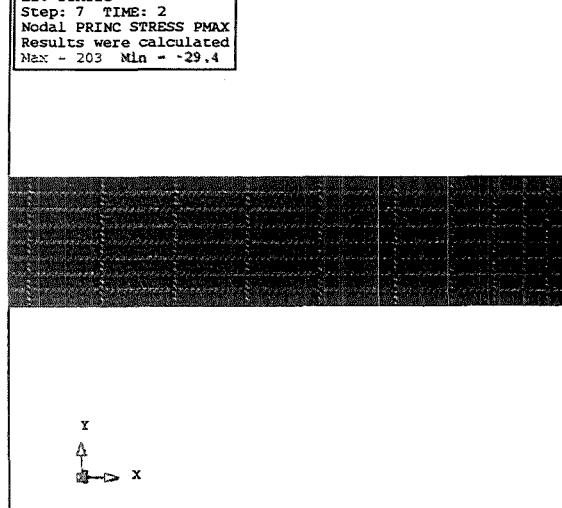
Model: CO07
 L2: STATIC
 Step: 7 TIME: 2
 Nodal PRINC STRESS PMAX
 Results were calculated
 Max = 203 Min = -29.4

After the brazing



Model: CO07
 L2: STATIC
 Step: 7 TIME: 2
 Nodal PRINC STRESS PMAX
 Results were calculated
 Max = 203 Min = -29.4

After the brazing



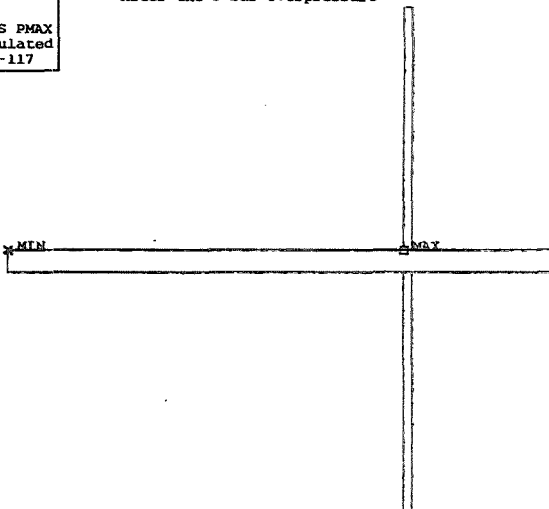
194
185
176
167
150
133
116
99
82
65
48
31
14
-2.58
-11.5
-20.4

1

2

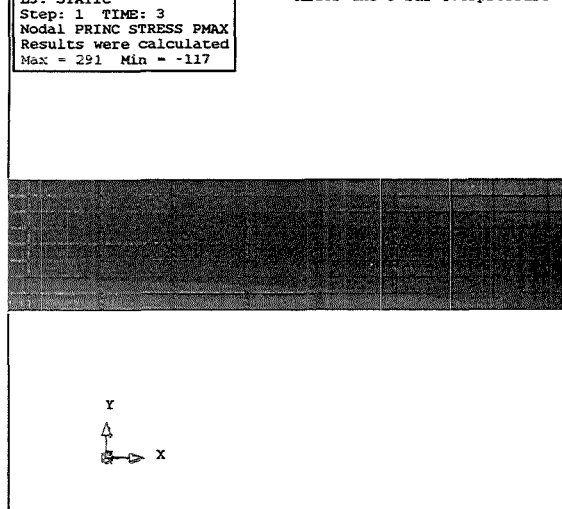
Model: CO07
 L3: STATIC
 Step: 1 TIME: 3
 Nodal PRINC STRESS PMAX
 Results were calculated
 Max = 291 Min = -117

After the 5 bar overpressure



Model: CO07
 L3: STATIC
 Step: 1 TIME: 3
 Nodal PRINC STRESS PMAX
 Results were calculated
 Max = 291 Min = -117

After the 5 bar overpressure



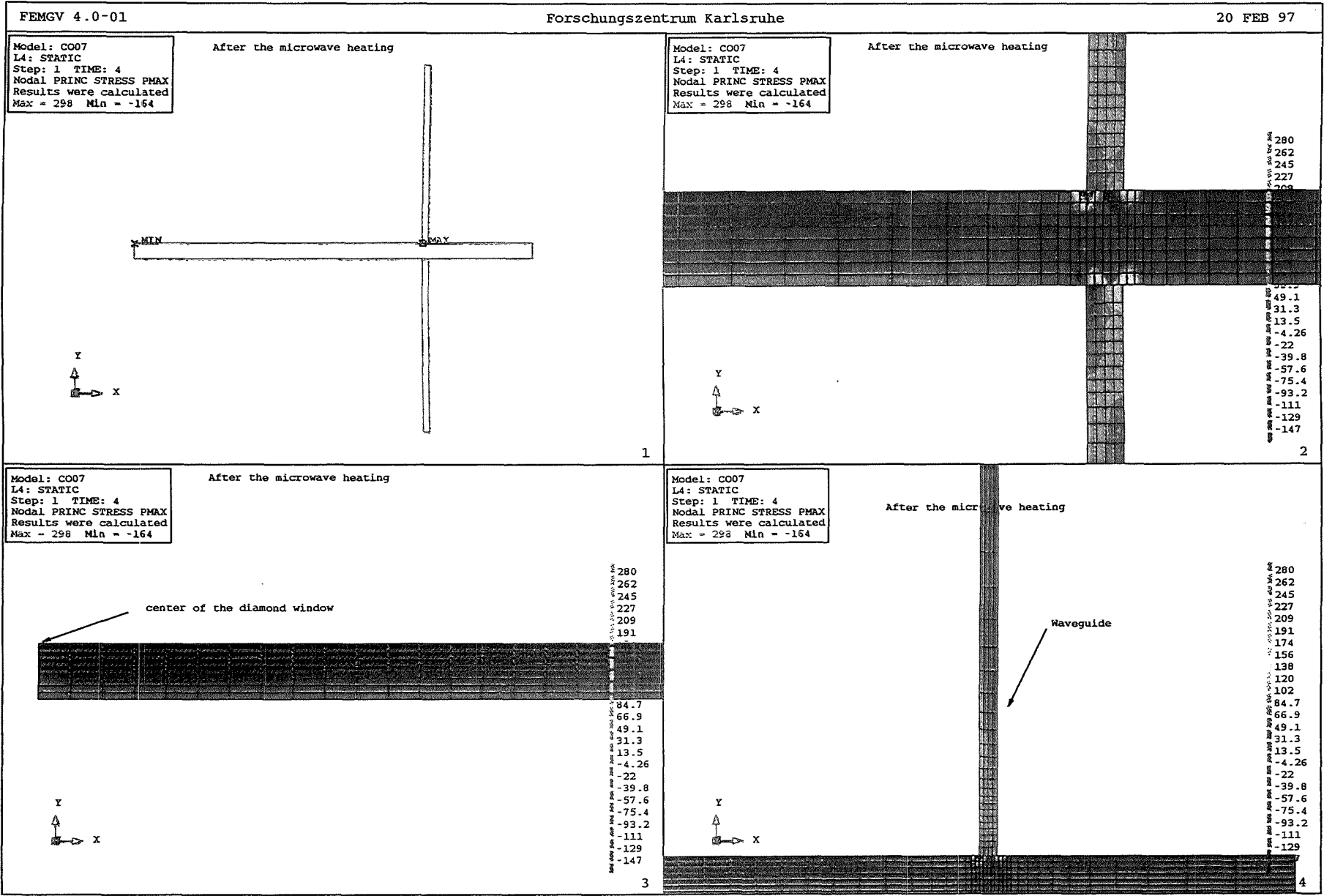
275
259
244
228
212
196
180
164
148
132
116
100
84
68
52
36
20
4
-12
-26
-40
-54
-68
-82
-96
-110

3

4

Fig. 11 Maximum and minimum stress of CVD-diamond disk after brazing and at 0.5 MPa (5 bar) static overpressure. 15

Maximum principal stresses (copper, 0.7mm, 20mm)



Maximum principal stresses (copper, 0.7mm, 20mm)

Fig. 12: Maximum and minimum stresses of brazed CVD-diamond disk under 0.5 MPa (5 bar) static overpressure and additional 1 MW mm-wave heating.

4. Design of Window Block

Figures 13 and 14 show a schematic 3D-view of the window block and cooling assemblies containing a flat 7x7 array of window units. The dimensions of the window block are approximately 1.5 m x 2.5 m x 0.7 m (Fig. 15). The window units can be isolated from the vacuum vessel and remotely removed without breaking vacuum by lip-seal welding (Figs. 16-18). The details of mounting and cooling of the CVD-diamond the disk are plotted in Figs. 19-21.

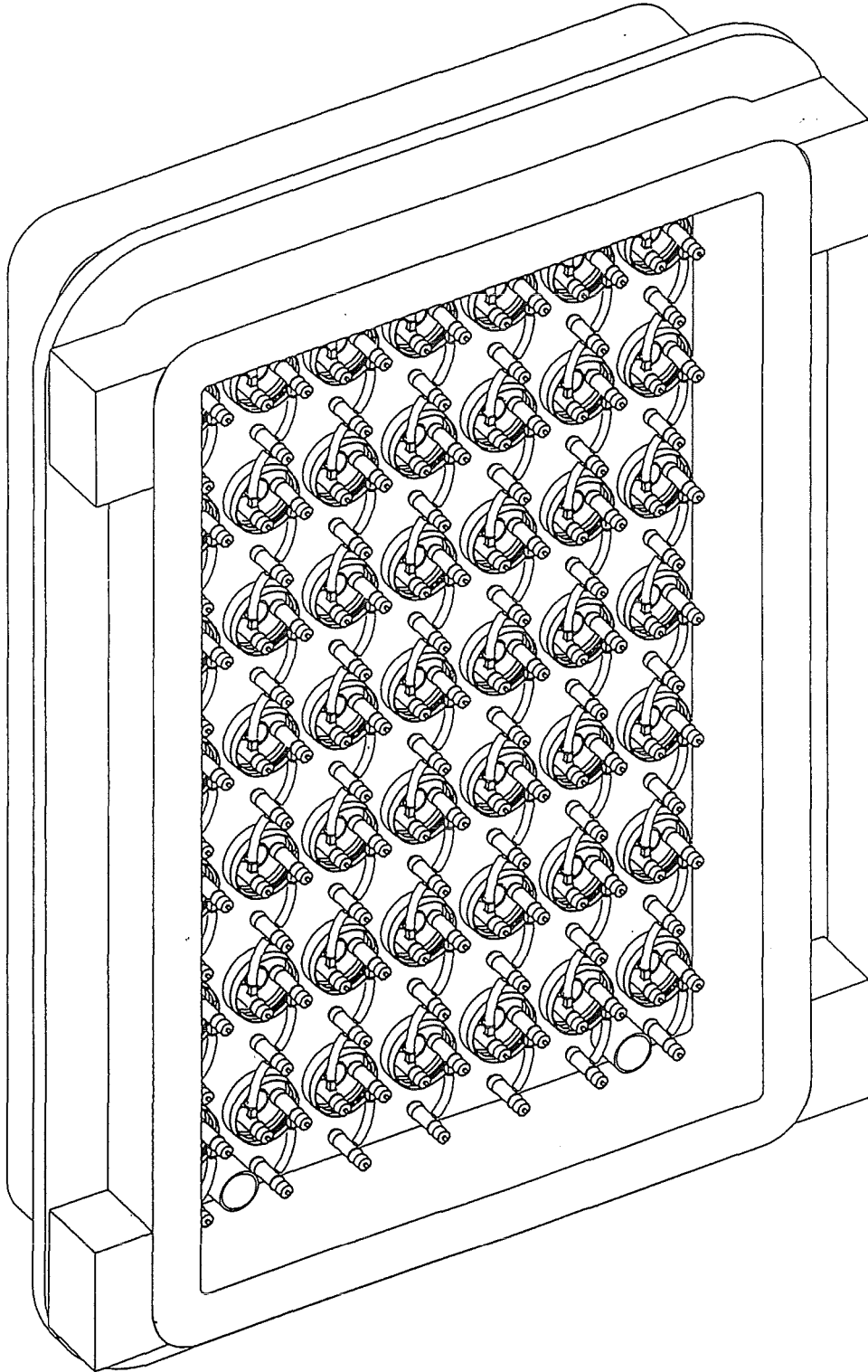


Fig. 13: Schematic 3D-view of the ECH window block.

DIMENSIONS RELATE TO ROOM TEMPERATURE (293K)

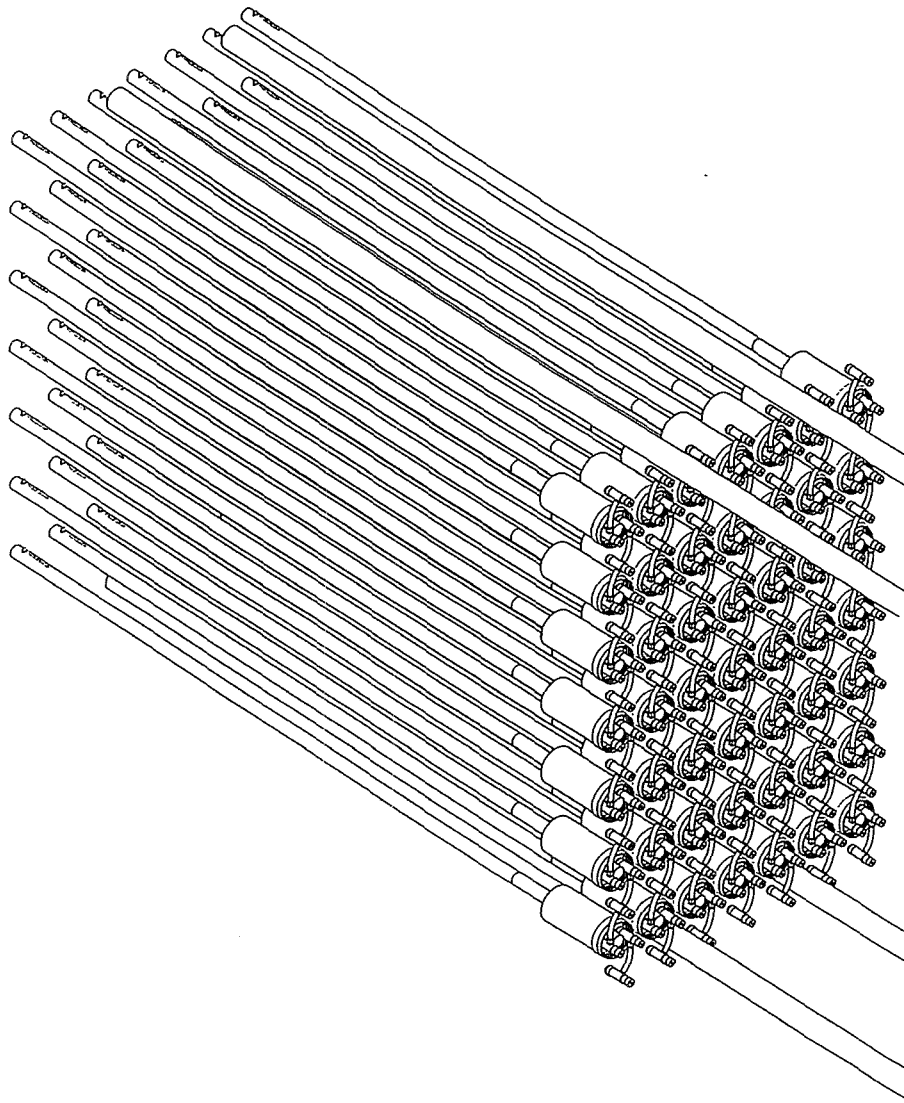
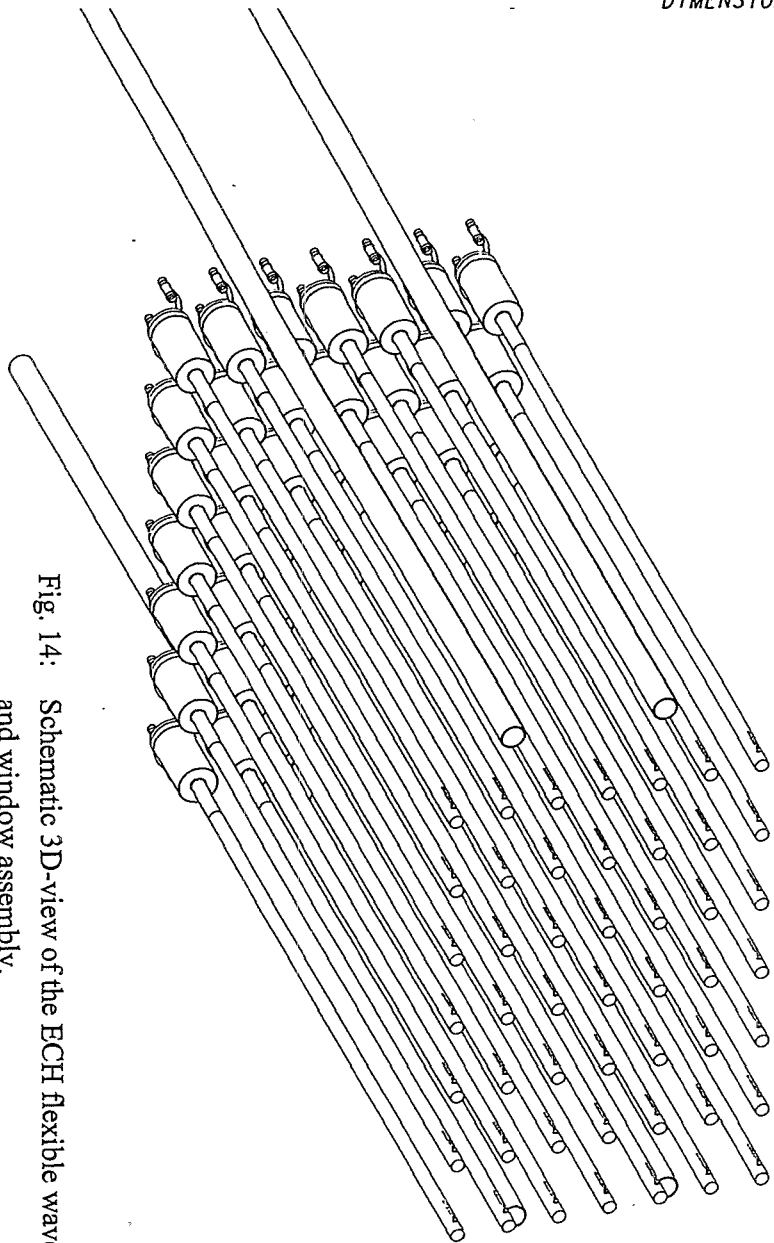
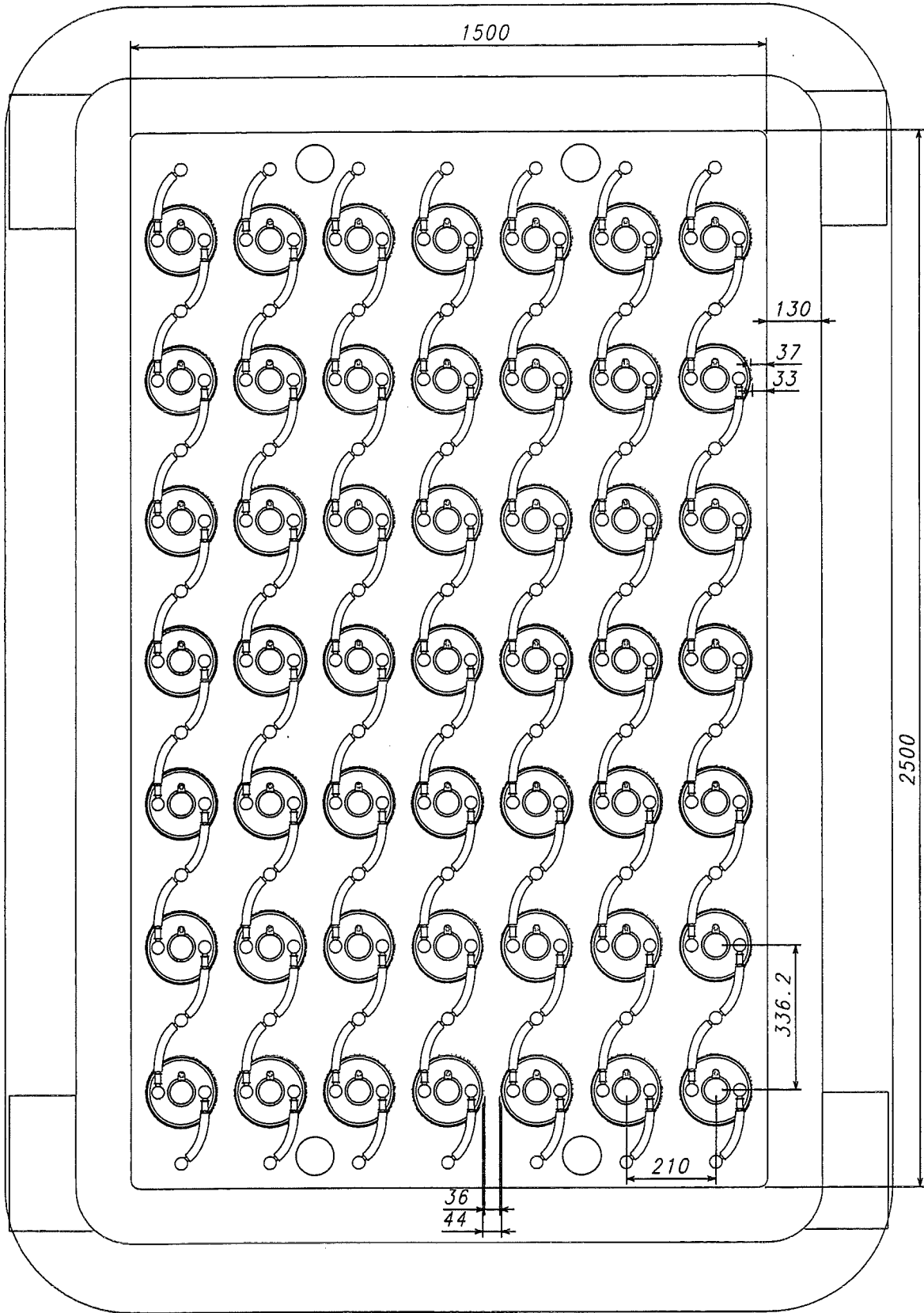


Fig. 14: Schematic 3D-view of the ECH flexible waveguides and window assembly.

TITLE ECH&CD FLEXIBLE WAVEGUIDES & WINDOW BLOCK ASSEMBLY		ORIG FRAME SIZE 840 x 594 DRAWN D.G. CHM'D D.O.U. BPD JGM JGM RESP. ENGR JWS CHM'D RESE. OTTA DATE 23-JUN-98 W.B.S. TITLE Work Breakdown Structure 5.2 BASELINE VERSION - W.B.S. TITLE Electron Cyclotron Heating & Current NAME OF ORGANISATION GARCHING JWS DO NOT TAKE MEASUREMENTS USE ONLY DIMENSIONS GIVEN	ITER-EDA NOT FOR PUBLICATION The information on this drawing is confidential under the terms of the ITER EDA agreement. This information shall not be transmitted to anyone else in any manner without the express written consent of ITER.	
THIRD ANGLE PROJECTION		DRAWING NUMBER 5210.07.510.00.1 2,0 0,0 3W-		

DIMENSIONS RELATE TO ROOM TEMPERATURE (293K)



NOTES.

1/. ALL DIMENSIONS IN millimetres UNLESS STATED

Fig. 15: ECH window and window cooling assembly at closure plate

TITLE ECH&CD WINDOW AND WINDOW COOLING WINDOW ASSEMBLY AT CLOSURE PLATE		DRG FRAME SIZE 420 x 594		ITER-EDA <small>NOT FOR PUBLICATION</small> <small>The information on this drawing is confidential under the terms of the ITER EDA agreement. This information shall not be transmitted to anyone who is not authorized to receive it</small>	
DATE 19-MAY-98	WORK BREAKDOWN STRUCTURE 5.2	DRAWN BPD	D.O. CHK'D JGM		
BASELINE VERSION -	W.B.S. TITLE Electron Cyclotron Heating & Current	RESP. ENGR MM1	JWS CHK'D -	RESP. OFFR MM1	NAME OF ORGANISATION CHINA
DO NOT TAKE MEASUREMENTS USE ONLY DIMENSIONS GIVEN	THIRD ANGLE PROJECTION	DRAW 5.2	NUMBER 07.60.00.05	OBJECT TYPE 2D	FORMAL REV 00
				WORKING REV 01	STATUS W ---

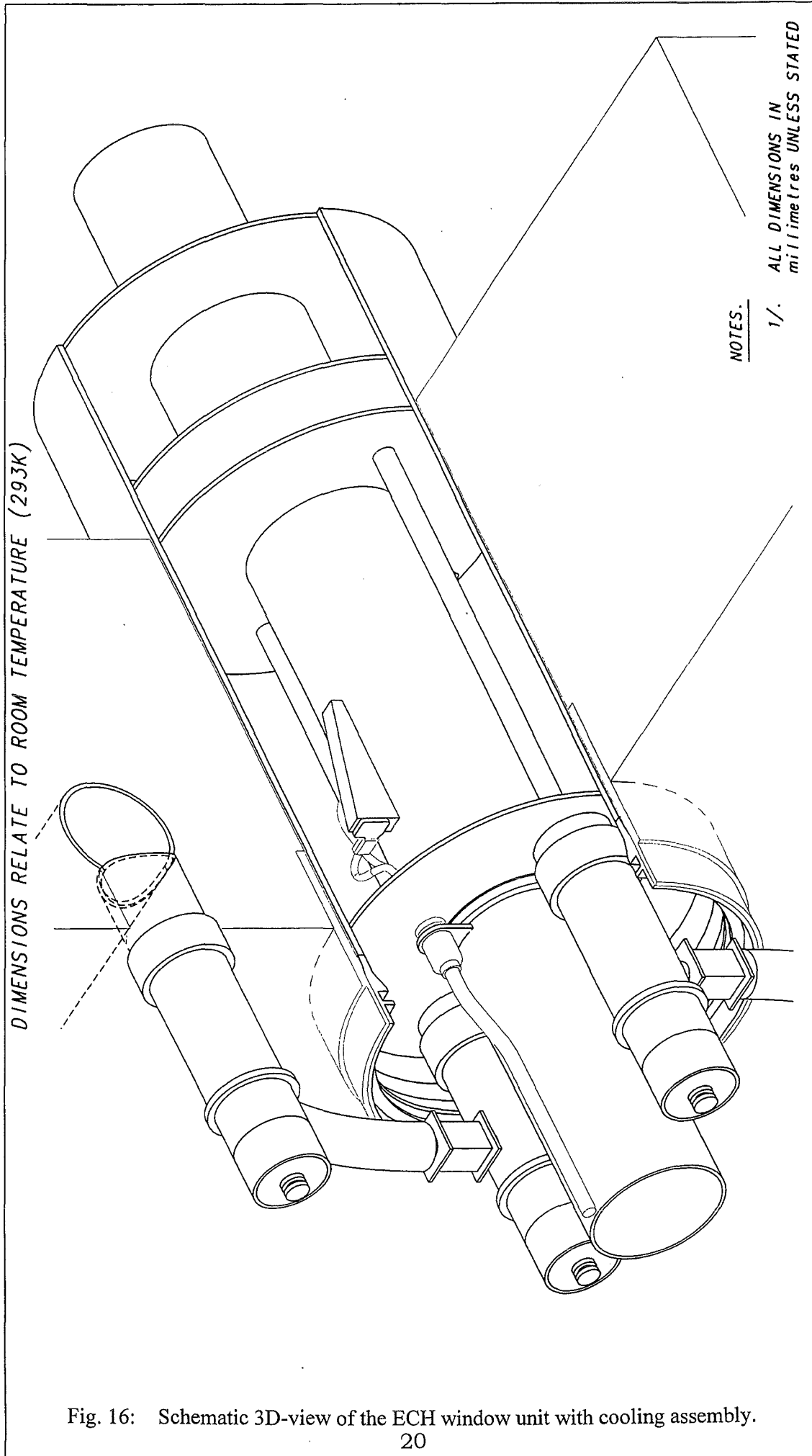


Fig. 16: Schematic 3D-view of the ECH window unit with cooling assembly.

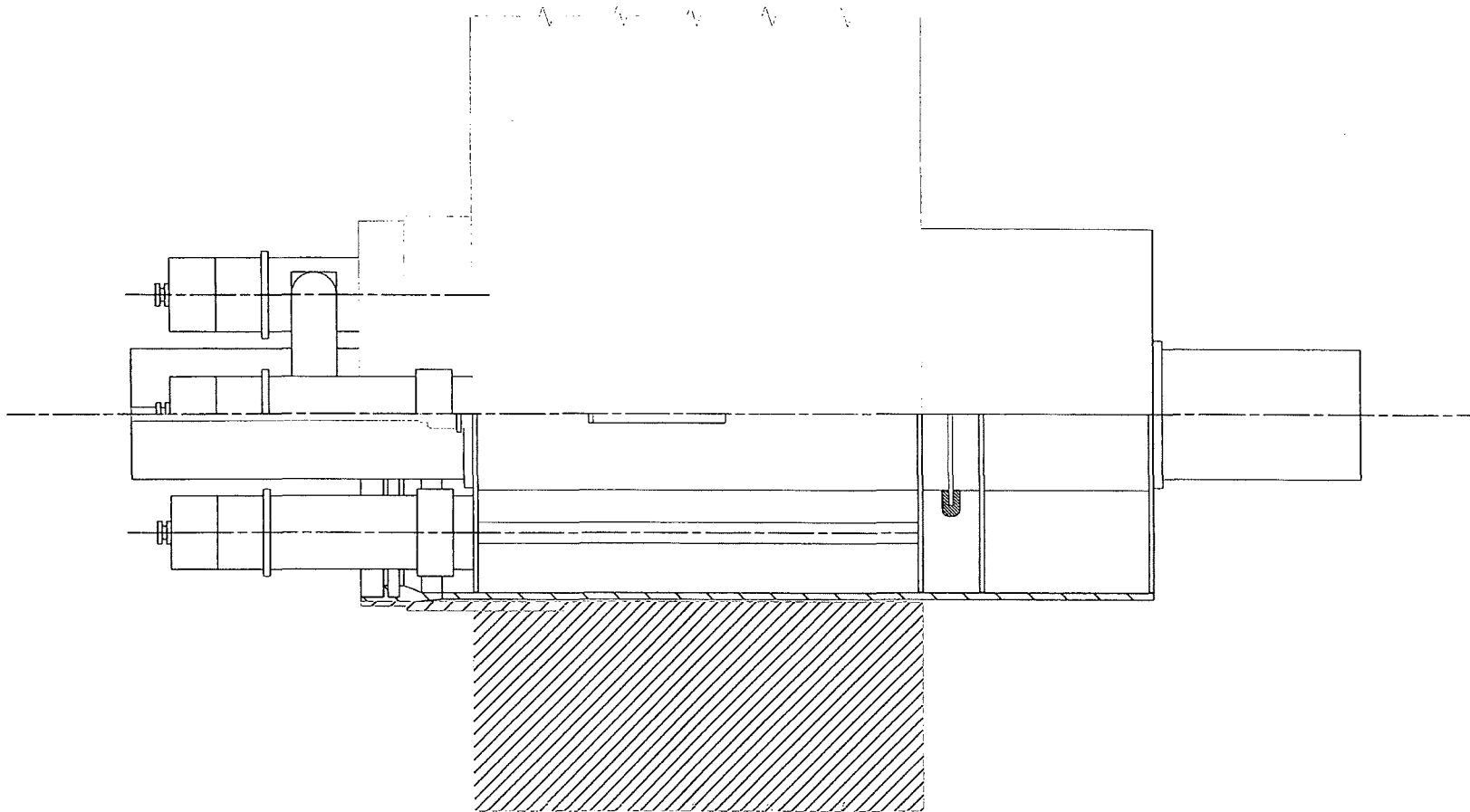


Fig. 17: Schematic top-view of the ECH window unit with cooling assembly.

21

0 20 100

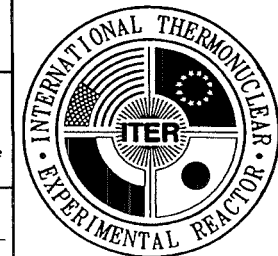
NOTES.

1/. ALL DIMENSIONS IN millimetres UNLESS STATED

TITLE <i>ECH&CD WINDOW AND WINDOW COOLING TOP VIEW</i>	
DATE <i>01-APR-98</i>	WORK BREAKDOWN STRUCTURE <i>5.2</i>
BASELINE VERSION <i>-</i>	W.B.S. TITLE <i>Electron Cyclotron Heating & Curren</i>
DO NOT TAKE MEASUREMENTS USE ONLY DIMENSIONS GIVEN	THIRD ANGLE PROJECTION

DRG FRAME SIZE <i>420 x 297</i>		
DRAWN <i>BPD</i>	D.O CHK'D <i>JGM</i>	D.O.M. <i>JGM</i>
RESP. ENGR <i>MMI</i>	JWS CHK'D <i>---</i>	RESP. OFFR <i>MMI</i>
NAME OF ORGANISATION <i>GARCHING JWS</i>		
DRAWING NUMBER <i>5.20.07.60.00.2</i>		

ITER-EDA			
NOT FOR PUBLICATION			
The information on this drawing is confidential under the terms of the ITER EDA agreement. This information shall not be transmitted to anyone who is not authorised to receive it			
OBJECT TYP <i>2D</i>	FORMAL REV <i>000</i>	WORKING REV <i>000</i>	STATUS <i>C---</i>



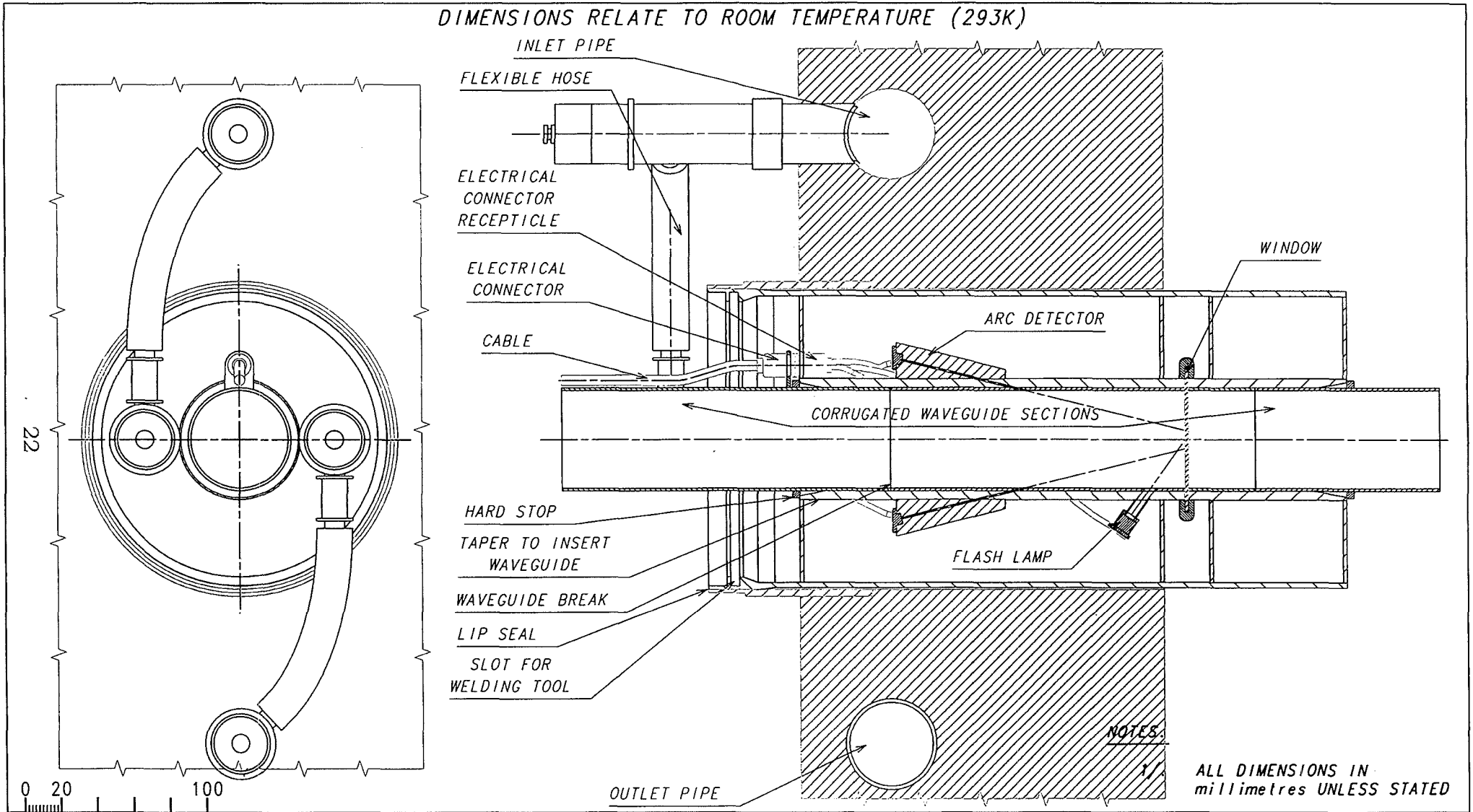
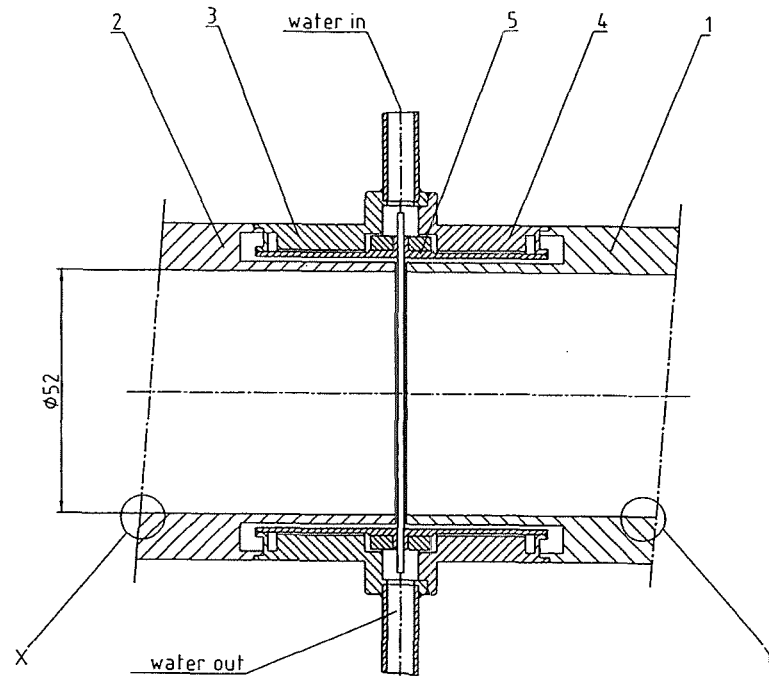
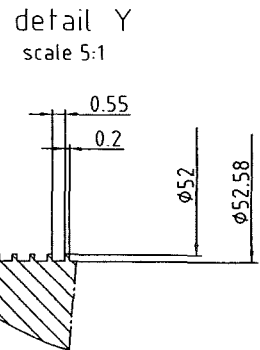
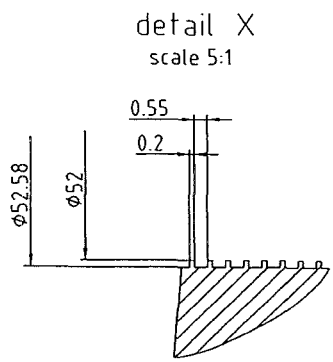


Fig. 18: Schematic cross-section of the ECH window unit and cooling assembly and optional arc detector with flash lamp tester

Fig. 19: Details of mounting and cooling of the diamond disk.



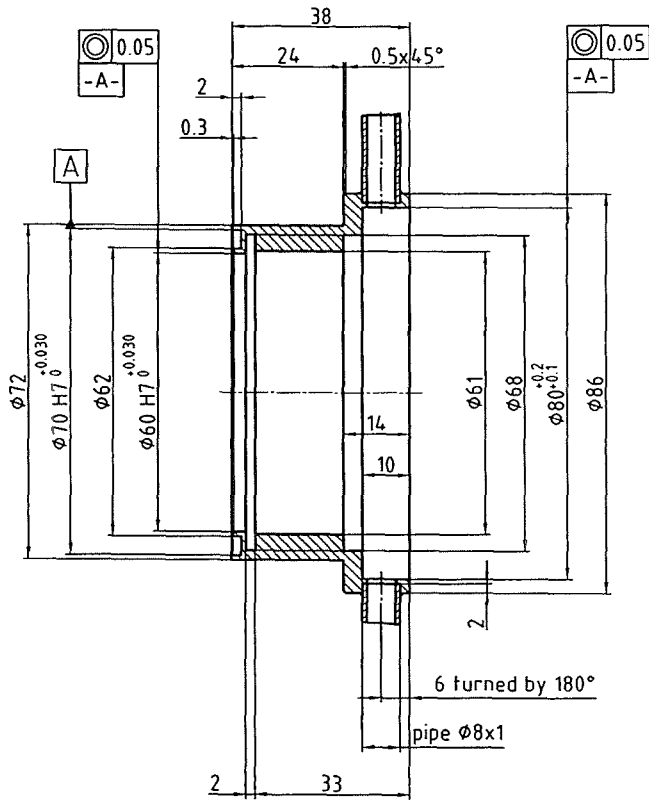
- 1 Waveguide section with arc detector
- 2 Waveguide section to plasma torus

Diese Zeichnung enthält die Rechte der Erfindung. Die Rechte der Erfindung sind durch das Patentamt geschützt. Die Rechte der Erfindung sind durch das Patentamt geschützt. Die Rechte der Erfindung sind durch das Patentamt geschützt.

Genius13-Datei: 01195.DWG
 Diese Zeichnung wurde mit CAD erstellt. Änderungen dürfen nur mit CAD durchgeführt werden.

Zulässige Freimaßtoleranzen in mm								DIN 7168 - mittel		F	Forschungszentrum Karlsruhe GmbH Inst. für technische Physik
0.5-3	3-6	6-30	30-120	120-400	400-1000	1000-2000	2000-∞				
+0.1	+0.1	+0.2	+0.3	+0.5	+0.8	+1.2	+2				
Maßstab	1:1	Gewicht						Werkstoff		Zeichnungs-Nr ITP-GY-523-3-BI	
								Tag	Name		
								Bearb.	16.07.1998		SZCZ
								Ges.			
								P.I.			
								Vorhaben		Blatt 1 Bl.	
								FE_IT_TH			
Zustand	Änderung	Datum	Name	Urspr.				Ersatz für:		Ersetzt durch:	

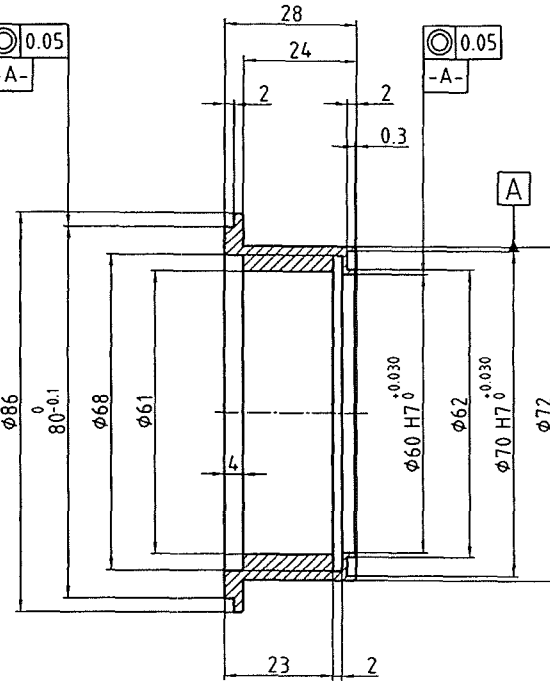
Fig. 20: Items 3 and 4 of Fig. 19.



Item 3
corners broken

Mat: VA

1/6



Item 4
corners broken

Mat: VA

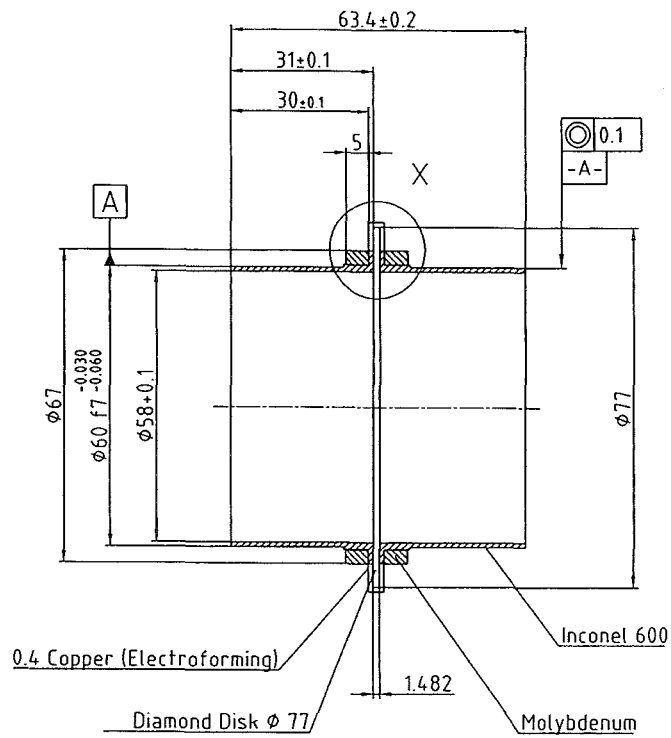
1/6

Diese Zeichnung ist Eigentum der Forschungszentrum Karlsruhe GmbH. Sie ist nur für den Zweck, für den sie erstellt wurde, gültig. Jede Vervielfältigung, Verbreitung oder Nutzung ohne schriftliche Genehmigung der Forschungszentrum Karlsruhe GmbH ist untersagt.

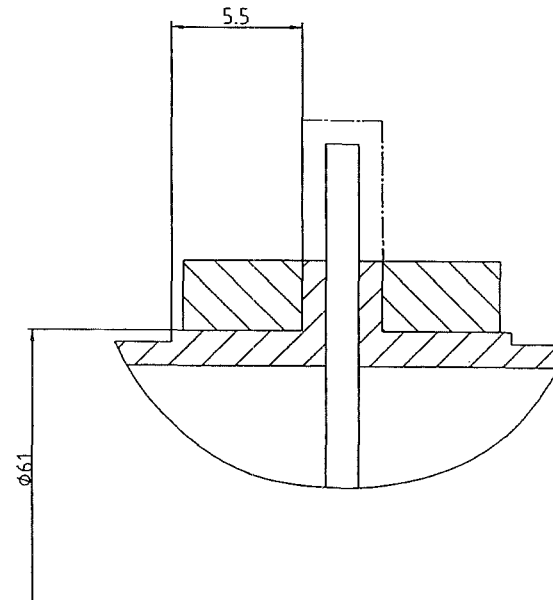
Genius3-Datei: 01195.DWG
 Diese Zeichnung wurde mit CAD erstellt. Änderungen dürfen nur mit CAD durchgeführt werden.

Zulässige Freimaßtoleranzen in mm		DIN 7168 - mittel		F	Forschungszentrum Karlsruhe GmbH Inst. für technische Physik
0,5-3	3-12	12-30	30-125		
±0,1	±0,1	±0,2	±0,3		ITER TORUS DIAMOND WINDOW
					Item 3,4
Maßstab 1:1	Gewicht	Werkstoff	Tag	Benennung	
			27.03.1998	SZCZ	
		Bearb.		ITER TORUS DIAMOND WINDOW	
		Gepr.		Item 3,4	
		Des.		Zeichnungs-Nr	
		P.I.		ITP-GY-523-3c	
		Vorhaben		Blatt	
		FE_IT_TH		1	
Zustand	Änderung	Datum	Name	Urspr.	Ersatz für:
					Ersetzt durch:

Fig. 21: Item 5 of Fig. 19 showing the encased cooling rim.



detail X
scale 5:1



Item 5
corners broken

1.6/

Genius13-Datei: 01195.DWG
Diese Zeichnung wurde mit CAD erstellt. Änderungen dürfen nur mit CAD durchgeführt werden.

Zulässige Freimaßtoleranzen in mm							
0,5	3	6	30	120	600	1000	3000
±0,1	±0,1	±0,2	±0,3	±0,5	±0,8	±1,2	±2

Maßstab 1:1		Gewicht		Werkstoff		DIN 7168 - mittel	
				Tag		Name	
				Bearb. 27.03.1998		SZCZ	
				Gepr.			
				Ges.			
				P.T.			
				Vorhaben		Benennung	
				FE IT TH		ITER TORUS DIAMOND WINDOW	
						Item 5	
				Zeichnungs-Nr		Blatt	
				ITP-GY-523-3d		1	
				Ersatz für:		Bl.	
				Ersatz durch:			

Diese Zeichnung ist Eigentum der Forschungszentrum Karlsruhe GmbH. Sie ist nur für den Zweck, den sie betrifft, zu verwenden. Die Weitergabe an Dritte ist ohne schriftliche Genehmigung der Forschungszentrum Karlsruhe GmbH untersagt. Die Haftung für Schäden, die aus der Verwendung dieser Zeichnung resultieren, ist ausgeschlossen.

Through the use of a double disk window, window failures can be easily detected (as on the JET LH and ICRH systems) even in the case that no arc detector with fiber optics light guides can be used in the nuclear environment. A very high vacuum ($\approx 10^{-7}$ Pa) can be achieved within the interspace between the two window disks. Since the total volume is small, vacuum pumping can be done with only one Vac-Ion pump. Any failure of either window is detectable as a pressure rise on the ion pump even in the case in which a lower case vacuum ($\approx 10^{-3}$ Pa) is present on the opposing surfaces. Bandwidth calculations show, that the disk distance should be e.g. 52.9 mm = 30λ . The resulting bandwidth is 3.0 GHz which is somewhat broader than for a single-disk window. Since the loss tangent and permittivity prove to be constant in the temperature range 70-370 K and because the thermal expansion of diamond is negligible, we have also constant reflection features of the diamond disks, so that there will be no problems of trapped power (no resonant cavity) between the two window disks. A double window is also good for lower tritium permeation.

The titanium ion getter pump should be a pump with 50 μ A ion pump current employing a 5 kV/1mA power supply (as in the JET LH system).

5. Cooling Modelling Experiments

In order to find the most effective cooling channel geometry for a water edge cooled CVD-diamond window assembly several tests on dummy windows have been performed. The two types of cooling circuits used for this reason are shown in Figure 22.

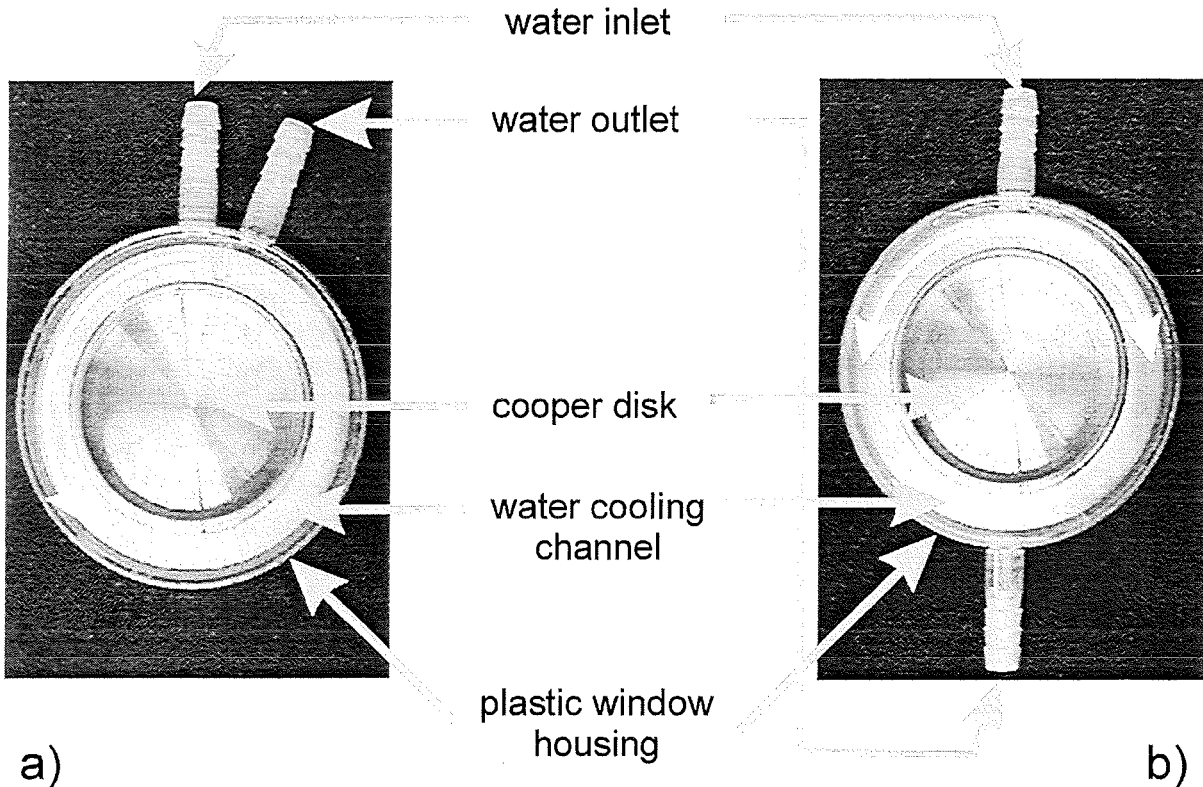


Fig. 22: Photograph of the two types of dummy windows.

- a) Enforced water flow circular around disk (FLB)
- b) Parallel water flow around window (FOB).

As a dummy window material a 5 mm thick and 100 mm diameter cooper disk was placed into two different window housings. The main difference of both assemblies is the shape of the cooling channel. One only enables a water flow in one direction around the disk rim (FLB) whereas the second one splits the water flow into two (hopefully) parallel streams (FOB). The mechanical realization of the first window assembly is more complicated due to the fact that a flow guiding component close to the edge of the disk is needed.

In a first series of experiments it was intended to determine the effective flow resistivity. Therefore the cooling channel of both windows had been supplied with water at a drift velocity of 7.7 l/min and a pressure of 3.6 bar. Table II summarizes the results.

window	ΔP [bar]
FLB	1.1
FOB	1.0

Table II.: Pressure drop determined for both windows.

In agreement with expectations the window assembly with the enforced circular water flow (FLB) shows a slightly higher pressure drop.

The second series of tests finally were performed to check the efficiency of the cooling system. Figure 23 shows a schematic drawing of the experimental setup.

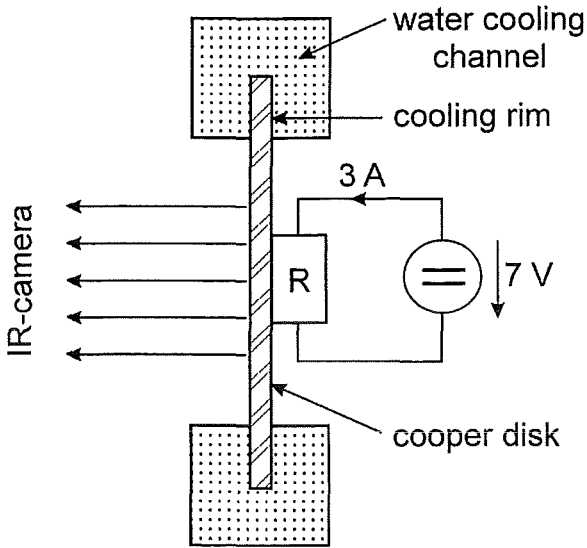


Fig. 23: Schematic drawing of window cooling experiment.

To simulate the heating of the window by a penetrating high power millimeter wave beam the center of the disk was heated on one side by electrical resistors. To monitor the center temperature increase the opposite side of the copper disk was scanned by an infrared camera. In dependence of various water flow rates the steady state temperature increase of both window assemblies has been recorded. The determined values as well as the fitted curves are shown in Figure 24.

As expected the window assembly with the enforced water flow around the window seems to provide a more efficient cooling at corresponding flow rates. The temperature offset of approximately 0.75 °C only can be explained by an asymmetrical flow around the window edge, which means that in half the cooling channel there is permanently a lower flow rate.

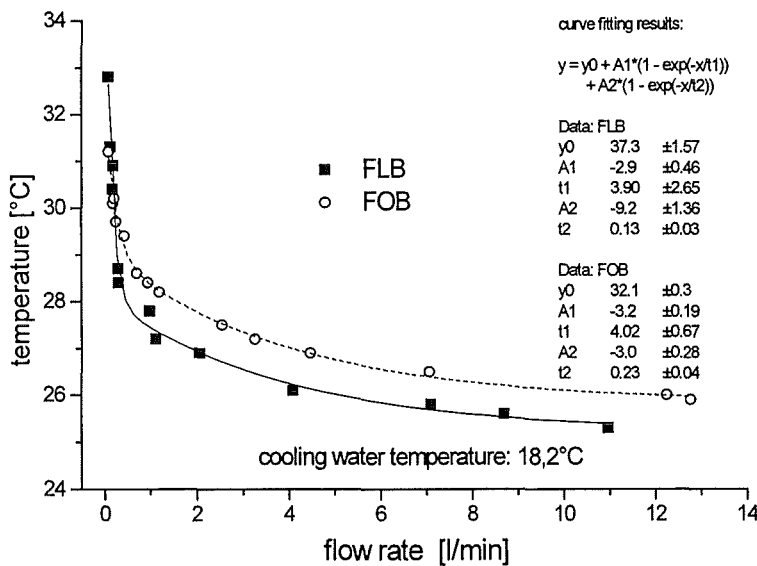


Fig. 24: Dummy window center temperature increase in dependence of the water flow rate.

After these first preliminary tests it seems that the window assembly with the enforced water flow circular around the disk bears some advantages:

1. More efficient water edge cooling due to a higher homogeneous water flow.
2. Easy failure detection due to the fact that the complete flow is affected in case of choking.

On the other side there are some negligible disadvantage:

1. Higher flow resistivity (easily can be compensated by a stronger pump).
2. More complicated mechanical design.

6. Broadband ECH Systems

A broadband transmission system is foreseen for the start-up system. Initially, a system based on step-tunable gyrotrons is being developed which will allow operation at up to six frequencies in the band 90-140 GHz (three frequencies for each of the two independent start-up systems). As there is still concern regarding the reliability of mechanical components of the heating and current drive ECH system in a nuclear environment, a graded design strategy is being followed. An alternative which simplifies the system through the elimination of the movable components at the expense of overall system performance. The alternative make use of step-tunable gyrotrons and fixed, rather than steerable, optics. In this case a coarse frequency adjustment (e.g. three discrete frequencies) can be used to provide control of the deposition location within the plasma. Most capability is retained with the exception of off-axis current drive where the efficiency is reduced and the ability for accurate localization is lost. Step tunability together with two fixed toroidal launch angles provides good performance in both the standard ignited and advanced regimes.

A design study for two different step-tunable 1 MW gyrotrons using diamond windows have been performed at FZK (Table III-IV). The first operating at 131.4 GHz, 150.7 GHz and 170 GHz could be used for heating and current drive applications, and the second, operating at 95.9 GHz, 114 GHz and 132 GHz, could be used for the start-up system. A proposal of the Japanese Home-Team for a tunable gyrotron for start-up considers a tube which operates at 86.1 GHz, 108.1 GHz and 129.9 GHz in the $TE_{19,5}$, $TE_{24,6}$ and $TE_{29,7}$ modes, respectively.

**Multi-Pass-Band Window for Step-Tunable Gyrotron
ITER Heating and Current Drive Gyrotron (CW)**

Frequency	131.4 GHz	150.7 GHz	170 GHz
Mode	$TE_{25,6}$	$TE_{28,7}$	$TE_{31,8}$
Diamond Window Thickness 3.34 mm	$7 \lambda / 2$	$8 \lambda / 2$	$9 \lambda / 2$

ITER Start-Up Gyrotron (CW)

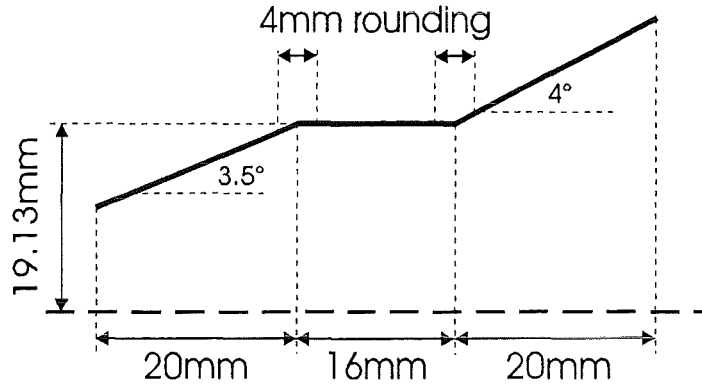
Frequency	95.9 GHz	114.0 GHz	132.0 GHz
Mode	$TE_{19,5}$	$TE_{22,6}$	$TE_{25,7}$
Diamond Window Thickness 3.31 mm	$5 \lambda / 2$	$6 \lambda / 2$	$7 \lambda / 2$

FZK Modelling Gyrotron (1 ms) with Single-Stage Depressed Collector

Frequency	117.9 GHz	140.1 GHz	162.2 GHz
Mode	$TE_{19,5}$	$TE_{22,6}$	$TE_{25,7}$
Fused Quartz Window Thickness 6.58 mm	$10 \lambda / 2$	$12 \lambda / 2$	$14 \lambda / 2$
Power (Eff.)	0.9 MW (36 %)	1.2 MW (45 %)	1.1 MW (39 %)

Tab. III: Proposed multi-frequency ECH systems for H&CD and start-up on ITER and results of modelling experiments at FZK.

I. CAVITY GEOMETRY



II. COLD-CAVITY RESULTS

	TE_{22,6}	TE_{19,5}	TE_{25,7}
frequency f (GHz)	113.988	95.927	132.033
diffractive Q_{dif}	796	584	1070
gaussian field length L_g (mm)	20.1	21.8	18.9
L_g / λ	7.64	6.97	8.32

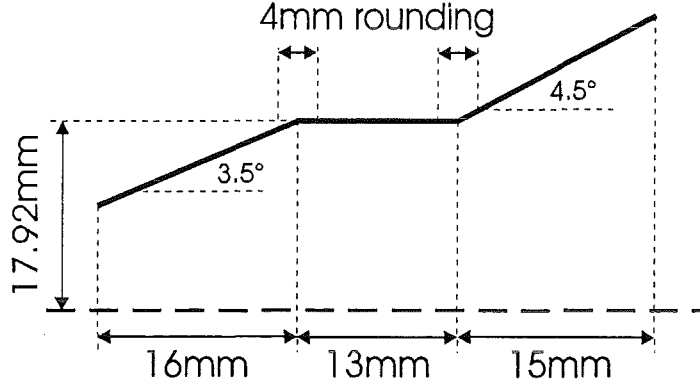
III. SELF-CONSISTENT RESULTS (DIODE GUN)

	TE_{22,6}	TE_{19,5}	TE_{25,7}
magnetic field B_0 (T)	4.48	3.72	5.28
beam voltage U_b (kV)	75	67	85
beam current I_b (A)	37	38	36
beam α	1.5	1.7	1.4
beam radius R_b (mm)	9.74	10.03	9.53
cathode voltage U_c (kV)	80.5	73.2	90
limiting current I_{lim} (A)	81	64	99
rms transverse velocity spread (%)	5	5	5
frequency f (GHz)	114.02	95.98	132.06
rf power w/o losses P_{rf} (kW)	1165	1180	1134
electronic efficiency η_{elec} (%)	42.0	46.3	37.1
peak wall loading ρ_{ohm} (kW/cm ²)*	0.91	0.71	1.15
ohmic losses P_{ohm} (kW)*	16	13	19
total quality factor Q_T	973	725	1293

* ideal cooper without wall roughness

Tab. IV: Preliminary study for a step-tunable gyrotron (with diode-type gun) at 114 GHz (TE_{22,6}), 96 GHz (TE_{19,5}) and 132 GHz (TE_{25,7}).

I. CAVITY GEOMETRY



II. COLD-CAVITY RESULTS

	TE_{31,8}	TE_{28,7}	TE_{25,6}
frequency f (GHz)	170.003	150.712	131.406
diffractive Q	1059	866	676
L_g / λ	9.35	8.54	7.88

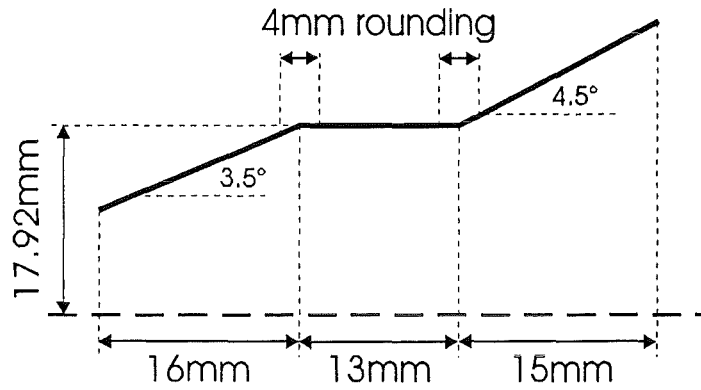
III. SELF-CONSISTENT RESULTS (DIODE GUN)

	TE_{31,8}	TE_{28,7}	TE_{25,6}
magnetic field B_0 (T)	6.73	5.93	5.13
beam voltage U_b (kV)	77	74	70
beam current I_b (A)	40	40	40
beam α	1.4	1.5	1.6
beam radius R_b (mm)	9.20	9.45	9.75
cathode voltage U_c (kV)	82.5	79.7	75.8
limiting current I_{lim} (A)	95	85	76
frequency f (GHz)	170.03	150.75	131.44
rf power w/o losses P_{rf} (kW)	1206	1206	1172
electronic efficiency η_{elec} (%)	39.1	40.7	41.9
peak wall loading ρ_{ohm} (kW/cm ²)*	1.60	1.37	1.14
ohmic losses P_{ohm} (kW)*	38	34	30
total quality factor Q_T	1326	1103	915
normalized field length μ	14.9	14.6	14.2
max rf power (kW)	1301	1317	1304
magnetic field (T)	6.700	5.905	5.105

* ideal cooper without wall roughness

Tab. V: Preliminary study for a step-tunable gyrotron (with diode-type gun) at 170 GHz (TE_{31,8}), 150 GHz (TE_{28,7}) and 131 GHz (TE_{25,6}).

I. CAVITY GEOMETRY



II. COLD-CAVITY RESULTS

	TE_{31,8}	TE_{28,7}	TE_{25,6}
frequency f (GHz)	170.003	150.712	131.406
diffractive Q	1059	866	676
L_g / λ	9.35	8.54	7.88

III. SELF-CONSISTENT RESULTS (TRIODE GUN)

	TE_{31,8}	TE_{28,7}	TE_{25,6}
magnetic field B_0 (T)	6.715	5.945	5.175
beam voltage U_b (kV)	75	75	75
beam current I_b (A)	40	40	40
beam α	1.5	1.5	1.5
beam radius R_b (mm)	9.20	9.40	9.65
cathode voltage U_c (kV)	80.9	80.7	80.4
limiting current I_{lim} (A)	84	86	89
frequency f (GHz)	170.05	150.76	131.44
rf power w/o losses P_{rf} (kW)	1207	1205	1192
electronic efficiency η_{elec} (%)	40.2	40.2	39.7
peak wall loading ρ_{ohm} (kW/cm ²)*	1.56	1.37	1.12
ohmic losses P_{ohm} (kW)*	37	34	29
total quality factor Q_T	1289	1102	892
normalized field length μ	14.4	14.5	13.4
max rf power (kW)	1391	1340	1245
magnetic field (T)	6.670	5.910	5.150

* ideal cooper without wall roughness

Tab. VI: Preliminary study for a step-tunable gyrotron (with triode-type gun) at 170 GHz (TE_{31,8}), 150 GHz (TE_{28,7}) and 131 GHz (TE_{25,6}).

Pilot experiments at FZK using a 1 ms gyrotron with an improved quasi-optical mode converter, single-stage depressed collector and fused quartz glass window ($12 \cdot \lambda/2 = 6.58$ mm thickness) gave 1.0 MW (41 % efficiency) in the $TE_{19,5}$ mode at 117.9 GHz, 1.2 MW (45 % efficiency) in the $TE_{22,6}$ mode at 140 GHz and 1.1 MW (49 % efficiency) in the $TE_{25,7}$ mode at 162.2 GHz [15].

The ultimate solution for a broadband window is the Brewster angle window. The Brewster angle for reflection free broadband transmission through a CVD-diamond disk ($\epsilon_r = 5.67$) is given by the expression

$$\theta_{Brewster} = \arctan \sqrt{\epsilon_r} = 67.21^\circ.$$

Thus, an elliptical diamond disk for a Brewster window in a HE_{11} waveguide with 52 mm diameter must have approximately the dimensions 149 mm x 77 mm. Current CVD capabilities allow to produce samples of up to 120 mm diameter and about 2mm thickness. Manufacturers claim that they also can produce high quality samples of up to 160 mm diameter in near future, so that such Brewster windows are becoming feasible. The schematic drawing in Fig. 25 shows the orientation of the Brewster window plate with respect to the polarization of the incident beam.

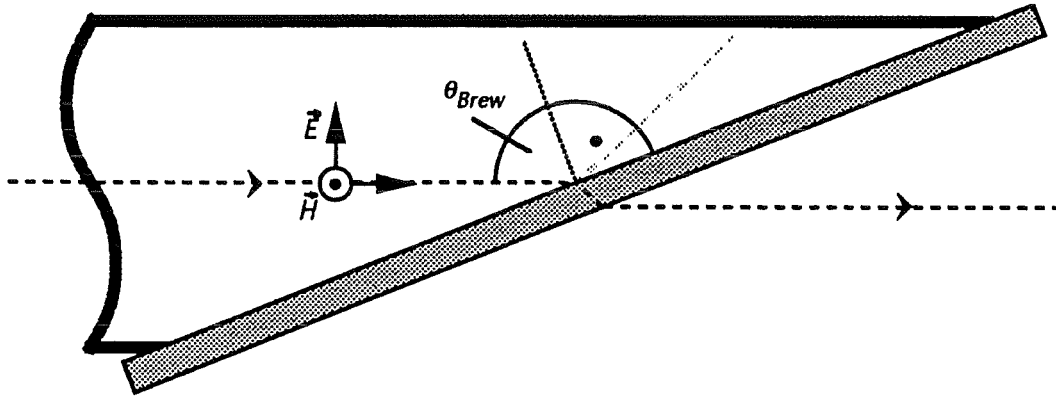


Fig. 25: Schematic drawing of a Brewster angle window.

First experiments at FZK with a conventional cavity gyrotron (pulse duration 1 ms) equipped with a prototype fused quartz glass ($\theta_{Brewster} = 62.87^\circ$) Brewster angle window gave approximately 1 MW output power for all operating mode series in the frequency range from 114 GHz to 166 GHz (frequency tuning in 3.7 GHz steps by variation of the magnetic field in the cavity) [15]. In Fig. 26 the results achieved with the Brewster window are compared to those measured by employing a conventional single-disk window. This window (thickness $d = 6.58$ mm; $12 \cdot \lambda_n/2$) has been optimized to have low reflections at least for a few number of frequencies (Table III).

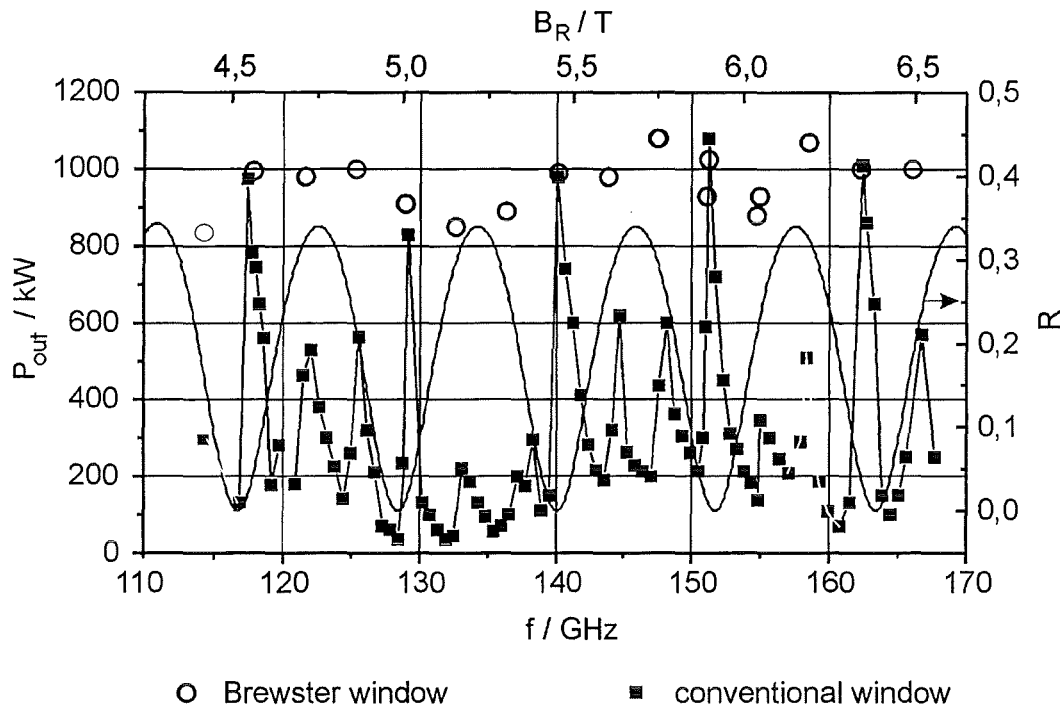


Fig. 26: Measured dependency of output power versus frequency for the two window concepts.

Due to the poor thermal conductivity of quartz glass ($k = 1.4 \text{ W/mK}$) a cooling system for the window assembly was of no use. In addition to this material specific problem the maximum dimensions for window plates available from the manufacturer had been limited to $215 \text{ mm} \times 95 \text{ mm}$. To be able to use such a plate as a Brewster window the clear window aperture had to be reduced from 100 mm diameter to 85 mm . To overcome these restrictions and in order to find a material which at least meets the requirements for a long pulse operation ($> 1 \text{ s}$) in a Megawatt millimeter wave beam further investigations on a Silicon-Nitride ceramic (Si_3N_4 from Kyocera: SN-287) have been performed. Since this material is available in arbitrary size and has its good thermal conductivity ($k = 60 \text{ W/mK}$) and mechanical strength, it was possible to realize a water edge cooled Brewster window with a desired clear window aperture of 100 mm in diameter. According to the Brewster relation the plate was mounted under an angle of $\theta_{\text{Brewster}} = 70.35^\circ$, which corresponds to a permittivity of $\epsilon_r = 7.85$.

After mounting the Si_3N_4 -Brewster angle window as the output window to the gyrotron the millimeter wave output power spectrum measured with the quartz glass Brewster window was reproduced almost identically [16].

By comparing the corresponding power levels measured with the conventional window to those obtained by using a Brewster angle window it was clear that even smallest window reflections ($< 1\%$) can have a significant influence on the gyrotron interaction leading to a change in the achievable maximum power level. As a consequence the reflection behavior of the required power detector also had to be taken into account. After turning the ballistic calorimeter in use for less than 2° another significant increase in output power and efficiency was reached. The results obtained for the three most relevant modes (pilot experiment) employing a single-stage depressed collector are listed below [17]:

mode	frequency	power	efficiency
$\text{TE}_{19,5}$	117.9 GHz	1.55 MW	48 %
$\text{TE}_{22,6}$	140.0 GHz	1.6 MW	60 %
$\text{TE}_{25,7}$	162.2 GHz	1.48 MW	57 %

Another advantage of the Brewster angle window assembly can be seen in Fig. 27. For minimal reflections in the conventional design the window plate has a resonant thickness with respect to the wavelength inside the material. This, of course, results in a local maximum of absorption given by the following formula:

$$A \approx \frac{\pi \cdot f \cdot d \cdot \tan(\delta) \cdot (1 + \epsilon_r')}{c_0}$$

where f is the resonance frequency, d is the plate thickness and c_0 is the velocity of light in vacuum. For a plate mounted at the Brewster angle each ray passes the window material only once, which results in the following equation:

$$A \approx \frac{2 \cdot \pi \cdot f \cdot \sqrt{\epsilon_r'} \cdot \tan(\delta)}{c_0} \cdot \frac{d}{\sin(\Theta_{Brewster})}$$

From these equations it is obvious that the amount of power absorbed in the conventional window, compared to that in a Brewster angle window of similar thickness, increases at a stronger rate with permittivity. Figure 28 shows the ratio of the two absorptivities as a function of the disk permittivity. It can be seen, especially for a sapphire disk, that the Brewster angle window could reduce the absorption by a factor of 1.6. In addition the RF spot size on the window is increased due to the oblique incidence. This results in a lower peak temperature and less critical thermal stress conditions.

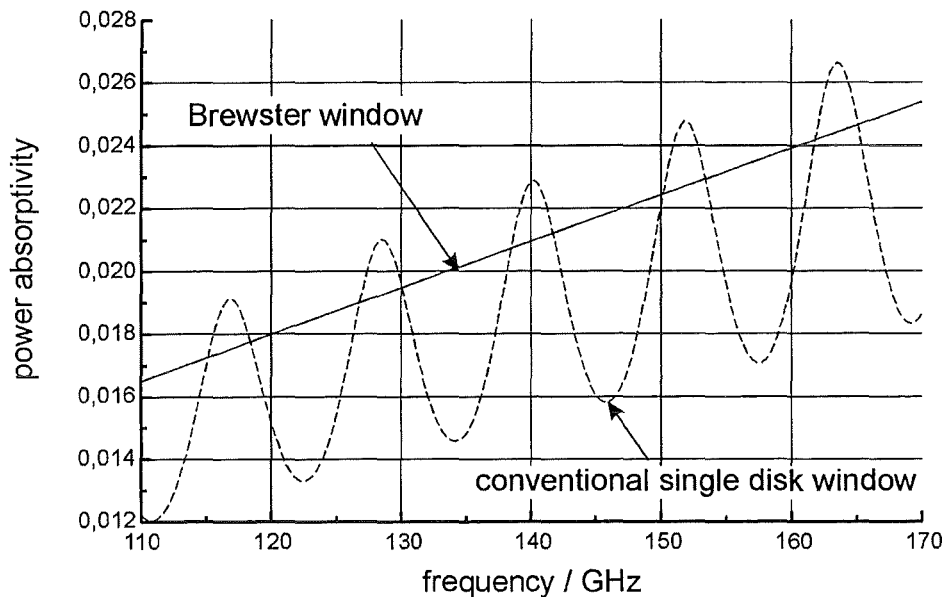


Fig. 27: Dependence of absorbed power in fused silica quartz glass windows ($d = 6.58$ mm) on frequency.

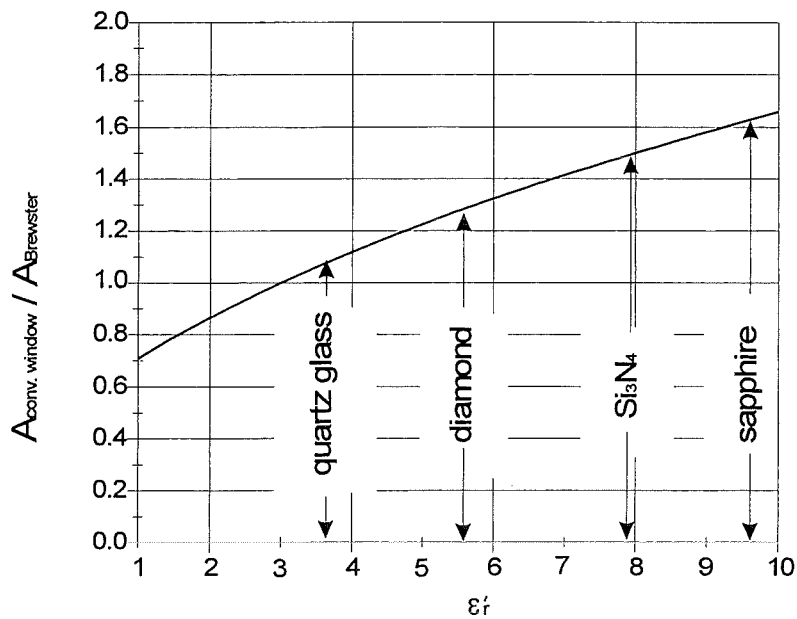


Fig. 28: Ratio of the absorptivities of conventional and Brewster window versus the permittivity.

The major benefits of the Brewster angle window – no reflections over a large frequency range – reduced absorption compared to the conventional window – lower thermal loading at the window – causes the drawback of a large, permittivity dependent Brewster angle and thus to enlarged window dimensions. To ease the computation of the Brewster angle isotropic window material is of advantage. The isotropy of the two relevant materials Si_3N_4 and fused quartz glass has been confirmed experimentally.

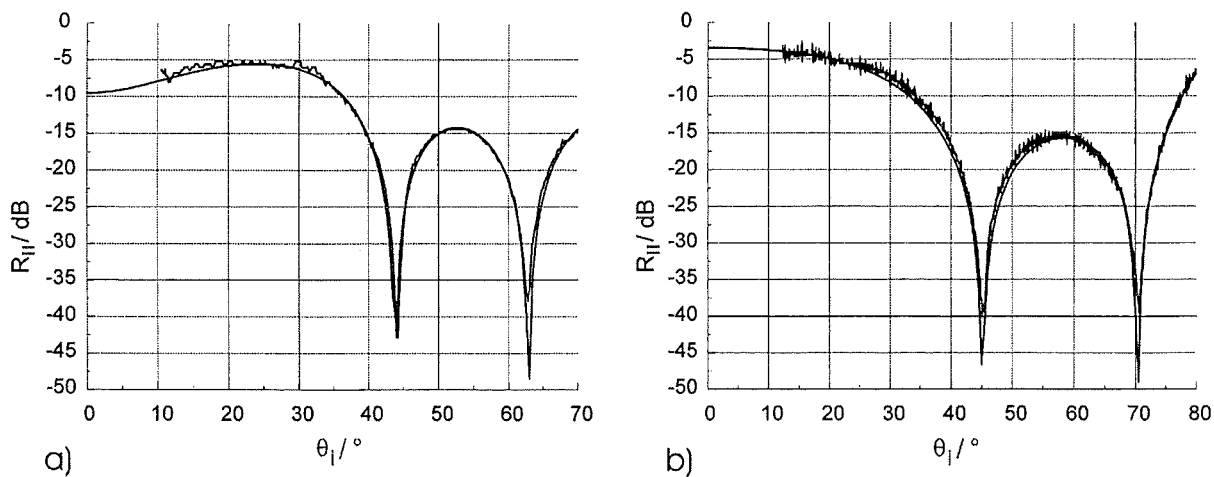


Fig. 29: Reflectivity in dependence of the angle of incidence measured and calculated at a frequency of 140 GHz in case of parallel polarization (\parallel):
 a) fused quartz glass plate, thickness 7 mm b) Si_3N_4 plate, thickness 3.16 mm.

Figure 29 shows the excellent agreement between the calculated (isotropic) reflectivities and the measurements at a frequency of 140 GHz. In agreement with theory, the window reflections vanish for parallel polarization at the Brewster angle of $\theta_{\text{Brewster}} = 62.87^\circ$ (Fig. 29 a) and $\theta_{\text{Brewster}} = 70.35^\circ$ (Fig. 29 b) for the fused quartz glass and the Si_3N_4 plate respectively.

Acknowledgments

This report is an account of work assigned as an ITER TASK to the European Home Team under the Agreement among the European Atomic Energy Community, the Government of Japan, the Government of the Russian Federation and the Government of the United States of America on Cooperation in the Engineering Design Activities for the International Thermonuclear Experimental Reactor ("ITER EDA Agreement") under the auspices of the International Thermonuclear Energy Agency (IAEA). The work was supported by the European Fusion Technology Program under the Projekt Kernfusion of the Forschungszentrum Karlsruhe. We gratefully acknowledge stimulating and useful discussions with Drs. R. Sussmann and J. Brandon from DeBeers Industrial Diamond Division Ltd. in Charters, UK. We also would like to thank very much our colleagues from JAERI, Naka, Japan, in particular Drs. T. Imai, A. Kasugai and K. Sakamoto for their excellent collaboration. Two of the authors, Prof. M. Thumm and Dr. O. Braz, were supported by the Deutsche Forschungsgemeinschaft (DFG 466 JAP-113/120/0).

References

- [1] Makowski, M., 1996, ECRF systems for ITER, IEEE Trans. Plasma Science, PS-24, pp. 1023-1032.
- [2] Makowski, M., 1998, Technology for electron cyclotron heating and current drive in ITER, Conf. Digest 23rd Int. Conf. on Infrared and Millimeter Waves, Colchester, UK, pp. 17-30.
- [3] Kerst, R. A., W. A. Swansiger, 1984, Journal of Nuclear Materials 122 & 123, 1499 - 1510.
- [4] Riehm, M. P., W. W. Scheltzer, D. A. Thompson, 1986, CFFTP-G-86041-Report.
- [5] Sussmann, R.S., J.R. Brandon, S.E. Coe, C.S.J. Pickles, C.G. Sweeney, A. Wasenczuk, A.J. Whitehead, C.J.H. Wort, C.N. Dodge, 1998, CVD Diamond: A new engineering material for thermal, dielectric and optical applications, Proc. Ultrahard Materials Technical Conference, Windsor (CDN), pp. 477-496.
- [6] Fünér, M., C. Wild, P. Koidl, 1998, Novel microwave plasma reactor for diamond synthesis, Appl. Phys. Lett., **72**, p. 1149.
- [7] Koidl, P., C. Wild, E. Wörner, W. Müller-Sebert, M. Fünér, M. Jehle, 1997, Optimization of diamond CVD for thermal and optical applications, Proc. 1st Int. Diamond Symposium, Seoul (ROK), 1996, p. 3.
- [8] Heidinger, R., R. Schwab, R. Spörl, M. Thumm, 1997, Dielectric loss measurements in CVD diamond windows for gyrotrons, Digest 22nd Int. Conf. on Infrared and Millimeter Waves, Wintergreen (USA), pp. 142-143.
- [9] Kasugai, A., D.C. Ballington, A. Beale, J.R. Brandon, O. Braz, T. Kariya, K. Sakamoto, R.S. Sussmann, K. Takahashi, M. Tsuneoka, T. Imai, M. Thumm, 1998, Chemical vapor deposition diamond window for high-power and long pulse millimeter wave transmission, Review of Scientific Instruments, **69**, pp. 2160-2165.
- [10] Thumm, M., 1998, Development of output windows for high-power long-pulse gyrotrons and EC wave applications, Int. J. of Infrared and Millimeter Waves, **19**, pp. 3-14.
- [11] Spörl, R., R. Schwab, R. Heidinger, V.V. Parshin, 1998, CVD Diamond for high power gyrotrons: Characterisation of dielectric properties, Proc. of ITG Conf. on Displays and Vacuum Electronics, Garmisch-Partenkirchen (D), ITG-Report No. 150, pp. 369-374.
- [12] Heidinger, R., R. Spörl, M. Thumm, J.R. Brandon, R.S. Sussmann, C.N. Dodge, 1998, CVD Diamond Windows for high power gyrotrons, Conf. Digest 23rd Int. Conf. IR & MM Waves, Colchester (UK), Invited Paper, pp. 223-225.
- [13] Spörl, R., R. Heidinger, C. Wild, R. Schwab, P. Koidl, 1998, Dielectric properties of CVD diamond for radiofrequency applications, Proc. 9th CIMTEC, Florence (I), in press.
- [14] Spörl, R., R. Heidinger, G. Kennedy, C. Brierly, 1998, Mechanical properties of free-standing CVD wafer, Proc. 9th CIMTEC, Florence (I), in press.
- [15] Braz, O., G. Dammertz, M. Kuntze, M. Thumm, 1997, D-band frequency step-tuning of a 1 MW gyrotron using a Brewster window, Int. J. Infrared and Millimeter Waves, **18**, pp. 1465-1477.
- [16] Dammertz, G., M. Kuntze, O. Braz, K. Koppenburg, B. Piosczyk, M. Thumm, 1998, 1 MW, 140 GHz gyrotron with Brewster window. Conf. Digest 23rd Int. Conf on Infrared and Millimeter Waves, Colchester, UK, pp. 276-277.
- [17] Kuntze, M., E. Borie, O. Braz, G. Dammertz, S. Illy, G. Michel, A. Möbius, B. Piosczyk, M. Thumm, 1998, Advanced high power gyrotrons for ECRH applications, Proc., 20th Int. Symp. on Fusion Technology (SOFT), Marseille, France, Vol. 1, pp. 485-492.